MINISTRY OF SCIENCE AND HIGHER EDUCATION
OF THE RUSSIAN FEDERATION
Federal state autonomous educational institution of higher education
“South Ural State University (National Research University)”
Polytechnic institute
Power engineering faculty
Industrial Heat Power Engineering department
Classifier number and the name of the Master's program
13.04.01 «Heat Power Engineering and Heat Engineering»

THESIS WORK
IS VERIFIED BY
Director
of Repair & constructions Ltd.

_____ K.A. Khasanov
«_____» _____ 2020

ALLOW TO DEFEND
Head of department
“Industrial Heat Power Engineering”
Candidate of technical sciences,
associate professor
_____ K.V. Osintsev
«_____» _____ 2020

P**acking density study on the metal powder particles used in 3D printing**

THESIS WORK OF THE MASTER'S PROGRAM
“HEAT POWER ENGINEERING”
SUSU-13.04.01.2020. 297.04.EN TW

Head of the Master's program,
Candidate of technical sciences,
associate professor
_____ K.V. Osintsev
«_____» __ _____ 2020

Head of work,
Grand PhD, professor
_____ A.A. Alabugin
«____» _____ 2020

Author of work,
Student of Master's program
of P-284 group
_____ S. Li
«_____» _____ 2020

Chelyabinsk 2020

ANNOTATION

S.Li. Packing density study on the metal powder particles used in 3D printing – Chelyabinsk: SUSU, PI, PEF; 2020, 66 p., 40 figure, references – 35, 9 slides of presentation

In TW the Discrete Element Method (DEM) was used to numerically simulate on the packing density of spherical particle with different size distribution, include analyze the effect of sphere stiffness, packing depth, container size on the packing density of the normally distributed spherical particles by the visual programming software PFC5.0. The dynamic characteristics and optimal parameters of the particle packing under different spherical model were obtained, and the spherical particles with normal distribution for particle size were physically experimented on the three-dimensional vibration test rig to obtain the density distribution under different vibration conditions.

TW purpose to discuss the high-density of metal powder particle packing in vary vibration condition with normal particle size distribution, further extensively study the packing density of metal powder particles, and improve the performance of metal 3D printing molding parts. The current problems are that the yield of finished products is not high, and the parameter design in the design process needs to be constantly optimized. There are many influencing factors for the product, and strict requirements for the process control of 3D printing are required. Market products for gas turbine blade precision, service life, maintenance way, put forward the more stringent requirements, efficiency of 3 D printing technology applied in leaf development and manufacturing, to adapt to the high reliability, high life, lightweight, low cost and rapid response to market demand, must quickly to advanced gas turbine blade manufacturing have a profound impact.

TW contains: Design, check and manufacture of 3D vibration table, learning and numerical simulation of particle flow discrete element simulation software, application and process analysis of metal powder 3D printing in turbine blade manufacturing. The application of metal powder 3D printing technology to the design and manufacturing of wind turbines can effectively shorten the design cycle, improve the flexible manufacturing technology of wind turbine blades, and greatly reduce the cost. SWOT-analysis of use of technology of the 3D printing for wind turbines is carried. Gantt's schedule of actions for implementation of technology for wind turbines is carried.

TABLE OF CONTENTS

ABSTRACT

The Discrete Element Method (DEM) was used to numerically simulate on the packing density of spherical particle with different size distribution, include analyze the effect of sphere stiffness, packing depth, container size on the packing density of the normally distributed spherical particles by the visual programming software PFC5.0. The dynamic characteristics and optimal parameters of the particle packing under different spherical model were obtained, and the spherical particles with normal distribution for particle size were physically experimented on the three-dimensional vibration test rig to obtain the density distribution under different vibration conditions. The purpose is to discuss the high-density of metal powder particle packing in vary vibration condition with normal particle size distribution, further extensively study the packing density of metal powder particles, and improve the performance of metal 3D printing molding parts. The numerical simulation results are verified. The research results are as following:

1. By analyzing the porosity change curve of particle packing with mean value of 0.3mm and variable variance, the result shows that with the increase of variance, the porosity tends to decrease firstly and then increase. In contrast to the packing density trend, the maximum value of packing density is 0.795 when the particle model with mean value of 0.3mm and variance of 0.2.

2. As for the spherical particles size with normal distribution, the porosity of particle in the packing container generally increases first and then stabilizes. When the stiffness value K is greater than 5e9, the growth trend is faster. The packing density finally tends to 0.346.

3. When the vibration condition is applied to the particle packing, there is an optimal matching parameter between the vibration frequency and amplitude, and for the particle with packing density, the larger the vibration frequency is, the smaller the corresponding matching amplitude parameter is.

The material in the blades of wind turbines can be eroded, a problem that affects the entire wind energy sector. 3D printing is the solution to the material problem. Erosion of the blade material due to rain, hail and dust has greatly reduced the life of wind turbines, which are expensive to replace and lose 2-4% of the value generated by wind power. In this paper, through the development of gant's chart, I reasonably arranged my task plan, and finally completed the research on metal powder 3D printing technology in turbine blades. For its specific application, its advantages and disadvantages are analyzed and compared through SWOT table, from which it can be seen that the design of 3D printing process parameters needs to be further improved and the performance of metal 3D printer is also required to be higher.

1 INTRODUCTION

1.1 Particle accumulation background

Particulate matter exists widely in our daily production and life with its colorful attitude. Whether it is mountains and rivers, boulders, or dust and smoke, it belongs to the category of particulate matter and has become the most commonly used substance except water by human beings [1]. Particulate matter in the human social development, the influence of the economic construction and the quality of life improve increasingly highlight, and involved in energy, chemicals, materials, building materials, light industry, metallurgy, electronics, weather, food, medicine, environment, space, and many other fields, particles is a very important cross discipline, much attention of research workers from all walks of life.

Particle materials have been widely and deeply studied [2], among which, metal powder particles play a pivotal role in metallurgy, chemical industry, materials, aerospace and other fields.

Granulometry is a science that studies the formation, morphology, performance, movement and change laws of particulate matter and engineering applications, which generally includes the characterization and measurement of particles, the preparation and treatment of particles, fluidization of particles, ultrafine particles, aerosols and the application of particle technology in various fields. Particle matter is also known as dispersions. Among the numerous studies on particles, particle accumulation has always been a very important research topic [3].

Particle accumulation phenomenon is widely existed in nature, and it is closely related to its related physical theory, scientific research, industrial and agricultural production and daily life, and has always been favored by scientists. Its application fields include chemical industry, agriculture, geological industry, food, medicine, metallurgy and so on. The problem of particle accumulation cannot be generalized and involves different scientific fields of macroscopic, mesoscopic and microscopic.

The application fields of particle accumulation mainly include: metallurgy, chemistry, chemical industry, materials field, scientific research, food engineering, medical engineering, aerospace industry, architecture, geology, transportation and agriculture. Metal powder particles mainly include single metal powder, alloy powder and some refractory compounds powder with metal properties.

Metal powder belongs to lose material, and general metal powder belongs to random loose material in the natural state. Its performance comprehensively reflects the properties of metal itself, the properties of individual particles and the characteristics of particle groups.

Generally, the properties of metal powder are divided into chemical properties, physical properties and technological properties. Chemical properties refer to metal content and impurity content; Physical properties include average particle size and particle size distribution, specific surface and true density of powder, particle shape, surface morphology and internal microstructure.

Process performance is a comprehensive performance, including powder fluidity,

bulk density, vibration density, compressibility, formability and sintering size change. Under the background of the era of intelligent manufacturing, 3D printing technology has gradually become a new engine to promote the development of manufacturing industry. Among them, 3D printing technology of metal has become a key research object for researchers due to its application advantages in aerospace, medical devices, precision instruments and complex component forming.

In metal 3D printing, high-energy laser beam through the step by step a molten metal powder to print out the final product, while the laser or electron beam has always been the focus of the study, but with the special equipment in the fields of aerospace, precision instruments, the improvement of metal components for 3 D printing performance requirements, alloy powder as basic elements gradually became the focus of attention.

During metal 3D printing, metal melting stage to obtain higher energy density of metal powder can improve the utilization rate of mechanical properties and forming metal parts, to improve the practicability of printout and comprehensive performance, if the density reach ideal level, can apply to print directly, after eliminating expended a lot of time consuming of the process, not only solves the problem of complex metal parts forming, but also a big milestone in mechanical manufacturing industry.

In the early stage, metal 3D printing manufacturers mainly relied on metal powder available in the market.

However, with the development of The Times and the progress of modern technology, higher and more special requirements have been put forward for the materials produced by metal powder particle manufacturers, and high-quality metal powder is needed as the raw material.

Metal powder particles can be prepared by reduction method, atomization method, electrolysis method, mechanical crushing method, hydroxyl method, and direct chemical method [4].

Among them, the powder produced by reduction method, electrolysis method and atomization method is widely used in powder metallurgy industry as raw material. However, the reduction and electrolysis methods are limited to the production of elemental metal powder, and they are not applicable to alloy powder. The most representative process is the formation of metal powder particles by gas atomization. Other methods include liquid atomization and centrifugal atomization.

The atomization method refers to the method of pulverizing molten metal into particles less than 150 um in size by mechanical means [5]. In the process of gas atomization, the molten metal passes through the narrow opening, just like the nozzle, and impacts with the gas phase when it is ejected.

The powder used for metal 3D printing is ball metal powder, which can guarantee the fluidity of powder particles and the performance of forming parts. Some high-melting metal powders can also be used for metal 3D printing.

The metal powder particles used in metal 3D printing are generally micron in size. Due to the particularity of the preparation process, the particle size of the metal powder particles produced by gas atomization method meets a certain distribution range, and the particle size differential distribution curve of the powder is unimodal, which is approximately normal.

1.2 Research status of particle density at home and abroad

Through the previous brief summary of the research field of particle accumulation, we can see its wide application and diversity, among which the density of particles is the most important for the study and application of particle accumulation.

1.2.1 Research direction of density

Scientists continuously explore various ways and methods to improve the particle accumulation density and study the physical characteristics of a large number of different particle accumulation.

In the late 1920s, Smith et al. [6] began to study the accumulation of spherical particles. With the development of the research and application of particle accumulation, the research on its density is more and more favored by the interdisciplinary researchers. Particle accumulation can be used as an effective starting point for the indirect study of the structure of various complex systems, and a good research model can be established for physicists and material scientists, such as: simple liquid system [7], amorphous solid or glass system [8], crystalline system [9], etc. Random accumulation of particles also has important scientific value in simulating simple liquids, amorphous metals and alloys, and many researchers have achieved success in practical implementation [10]. The regular arrangement of hard spheres is mainly used to study the crystallization process and crystallization dynamics of crystals.

The study on densification of particle accumulation can be roughly summarized as the following:

1. main factors affecting particle density;
2. how to obtain the optimal experimental parameters of density;
3. how to predict particle density;
4. how to characterize the macroscopic and microscopic characteristics of particle accumulation;
5. mechanism of particle accumulation densification.

For the study direction of all listed above, how to get the best density of experimental parameters and how to characterization of macroscopic.

1.2.2 Physical experiment methods

Experimental study of particle accumulation generally refers to the study of the accumulation of different particles under different containers under laboratory conditions, and the detection of the internal structure of particle accumulation by means of CT technology [11].so as to obtain the properties of particle accumulation.

The accumulation and flow of particles in containers [12], the influence of mechanical vibration on particle accumulation in cylindrical containers [13], etc., have been explored and studied by researchers through experimental methods. The particle packing density process generally goes through three stages: random loose packing, secret packing and ordered packing.

In 1656-1657, Huygens of the Netherlands first proposed the theory of physical pendulum. At the beginning of the 20th century, the problem of mechanical vibration was mainly focused on avoiding resonance. In 1921, h. holzer of Germany proposed a method to calculate the natural frequency and mode of torsional vibration of shafting. In 1930s, the study of mechanical vibration began to develop from linear vibration to nonlinear vibration. Since the 1950s, the study of mechanical vibration has developed from regular vibration to random vibration. Due to the development of automatic control theory and electronic computer, the calculation of multi-degree-of-freedom system which was considered very difficult in the past has become an easy problem to solve. With the development of vibration theory and experimental technology, vibration analysis has become an important tool in mechanical design.

In the research field of rock and soil and other loose bodies, the early application of mechanical vibration technology is mainly limited to the dense foundation engineering. For example, when the soil is excited by dynamic load, the friction between soil particles drops dramatically and the inter-pore pressure rises rapidly, resulting in the suspension or flow state of soil particles, which is called the "vibration liquefaction" phenomenon of soil [14]. When the vibration frequency of dynamic load is equal to or close to the natural frequency of soil particles, the phenomenon of "vibration liquefaction" of soil is most obvious.

Mechanical vibration refers to the regular reciprocating motion of an object or particle near its stable equilibrium position. The principle is that the strength of the vibration is measured by the amount of vibration, which can be the displacement, velocity or acceleration of the vibration body. Mechanical equipment working on the principle of vibration can produce the expected vibration and then realize the expected experimental conditions. In the field of mechanical engineering, in addition to the solid vibration, there are fluid vibration, and solid-fluid coupling vibration. The vibration test of solid particles is a kind of vibration coupling between solid and fluid.

As early as 400 years ago, Kepler predicted that the maximum packing density of a hard sphere of the same size in the universe would not exceed 0.74, that is, the packing density of FCC (face centered cubic) structure or HCP (hexagonal close packing) structure, which has been proved mathematically [15]. Bernal et al. pioneered this aspect in physical experiments, and the research results showed that the random accumulation of identical spheres could provide a useful model for the study of ideal simple liquids. Scott found that the upper limit of random packing density of 20,000 steel balls with diameter of 3.175mm in the rigid container could reach 0.63. Owe Berg et al. [16] dumped 5,000 steel balls with a diameter of 3.175mm into a cylindrical container with a diameter of 63mm, then supplemented by 3D vibration, and found that the arrangement formed was an ordered structure of dense square and six rows of HCP, with the corresponding packing density close to 0.74. 2009, An Xi Zhong et al. [17] for a dollar and binary sphere particles under the condition of vibration of dense packing experiment, compared with the overall charging is verified, batch feeding way the particle density higher, through a single sphere particle sizes in the accumulation of two-dimensional vibration under the condition of experiment, get the biggest bulk density was 0.7131, close to the theoretical value of 0.74, largest showed that two-dimensional vibration than the one dimensional vibration can

more effectively to realize the densification accumulation of particles; The maximum packing density of binary particles is 0.7522, which indicates that densification packing of binary particles with higher density can be realized under one-dimensional vibration condition. In 2015, after more in-depth research, li chao, etc on the dual dimensions of a peacekeeping three-dimensional vibration accumulation densification experiment [18], it is concluded that binary size ball in one dimension, two vibration under the condition of two-dimensional maximum density obtained from the corresponding optimum technological conditions for: 1 d vibration frequency 130 rad/s, volume fraction of 0.7, the particle diameter ratio r = 0.0654, extrapolation to get maximum density is 0.8294; 3D vibration, frequency is 110Rad/s, volume fraction is 0.7, particle size ratio r=0.0654, and the maximum density obtained by extrapolation is 0.8809. In 2015, An Xizhong and li chao et al. carried out an experimental study of binary mixed ball particles on a three-dimensional vibration table [19], and obtained the maximum density of 0.88.

To sum up, one yuan, binary sphere particles in a one-dimensional, two-dimensional and three-dimensional vibration conditions, with the method of batch charging, it is concluded that the general density, and the triple sphere particles density topological analysis and characterization, but the lack of corresponding physics experiment validation and characterization of quantitative, therefore, three yuan even more diverse sphere particles density remains to be further research. This topic in the existing experimental research on particulate matter density, on the basis of the field of 3 D printing for metal sintering of metal powder density remains to be further improve the problem, by the prevalence of particle size is approximate normal distribution of micron grade sphere particles in physics experiment, its density is experimental research, and indicates that the experimental parameters affecting the density and the optimum parameters of the vibration.

1.2.3 Numerical simulation method

1.2.4 Summary

The MC method does not need to assume the velocity distribution function of particles, and can be used to calculate some more complex particles. However, all particles involved in this topic are assumed to be spherical particles, so its advantages are not obvious in this topic. Compared with monte carlo method, molecular dynamics method and monte carlo method have higher accuracy and effectiveness in the calculation of macroscopic properties. However, since the motion state of each particle needs to be traversed, the amount of computation needs to be provided in the use of MD method is large, and the calculation process is very tedious, which requires high performance of the computer. The research core of this paper is metal particles with normal particle size distribution. It is necessary to establish a spherical powder particle model with normal distribution for numerical simulation, involving a large number of three-dimensional spherical particles with complex and diverse particle size distribution. It is concluded that the MD method is not suitable for the research of this subject due to its large amount of computation and complicated calculation process. Although MC method can be used in combination, it further increases its complexity.

Discrete element method using the dynamic relaxation method, Newton's second law and time step iteration each particle's movement speed and displacement, and is especially suitable for solving nonlinear problem, at the same time, by changing the particle and the boundary of analysis model, the contact mechanics model and parameters, can also analysis the contact between different medium particles with different boundary and its effect on medium particle movement.

To sum up, it is not only applicable to the physical model involved in this subject to obtain the dynamic characteristics of the internal particles in the vibration state, but also more conducive to the analysis of the boundary influence in the vibration process. In summary, this paper mainly USES the discrete element visualization programming software to simulate the metal sphere particles with normal particle size distribution.

1.3 Innovative points of the paper

The innovation of this paper mainly includes the following three parts:

First: the innovation of selecting the complexity of the research object.

For particle accumulation of research, both in physical experiment and numerical simulation of the physical and mathematical model and the deduction, even have lots of scientific research workers have done a lot of detailed research, and a lot of effective results, for example: one yuan diameter sphere particles such as physical model has been given, the theoretical maximum density value is 0.74, the binary and ternary sphere particles and the physical model is also given.

Yet for normally distributed particle size of sphere particle physics and the establishment of the mathematical model and the deduction is rare, investigate its reason, mainly lies in the size distribution of the model established after the uncertainty and random distribution of sphere particles position uncertainty, lead to can't accurately the establishment of a unified approximate density analysis solution for physical modeling and mathematical model. Since it is impossible to derive the exact value of the most approximate density theoretically, the most direct method is to conduct the analysis through physical experiments.

Second, numerical simulation was carried out for sphere particles with normal particle size distribution.

A large number of researches on the density of spherical particles focus on the physical experiment and numerical simulation of unary and binary spherical particles. For the numerical simulation study has been part of the triple sphere particles, the density is 0.81, however, the corresponding physical experiment research is very few, the reason can be roughly summed up in the triple sphere of as follows:

1. experiment particle size difference is large, and there is a specific proportion relationship, triple sphere particles ideal proportion of large, medium and small particle size for a 1-0. 41422:0.22474, the actual selection particle size as well as the preparation is difficult;

2. the particles with the smallest particle size in the ternary sphere have poor fluidity, which makes it difficult to fill the pores effectively, resulting in unsatisfactory experimental results;

3. because of the triple sphere particles in the same and accumulation conditions, the dense structure can be different, including three accumulation of face-centered cubic crystal and three accumulation of body centered cubic crystal, therefore.

Third: to establish more appropriate ways and methods to characterize microscopic characteristics.

Since the object of this study is spherical particles with normal particle size distribution, compared with the previous spherical particles with unitary, binary or ternary particle size, many existing methods of characterization of microscopic characteristics need to be re-examined, and the inapplicable feature description needs to be abandoned. At the same time, compared with previous scientific research achievements, the characteristics of the research object of this subject vary greatly, so it is necessary to describe the microscopic characteristics in a more appropriate way and method to adapt to and reflect the microscopic characteristics of spherical particles with normal particle size distribution. There are few precedents in this regard, so it is of great challenge and innovation.

1.4 Research significance

In the process of metal powder preparation, the powder particles will take on different shapes with different preparation methods, such as sphere, sub-sphere, polygon, porous sponge, and dendritic.

The breakthrough of low-cost preparation technology of metal powder for 3D printing has become an urgent problem for researchers at home and abroad. In recent years, domestic and foreign enterprises have invested a lot of capital and technical strength in the field of 3D printing metal powder preparation, and have made some progress, Figure 1.1 shows SLM working schematic diagram.

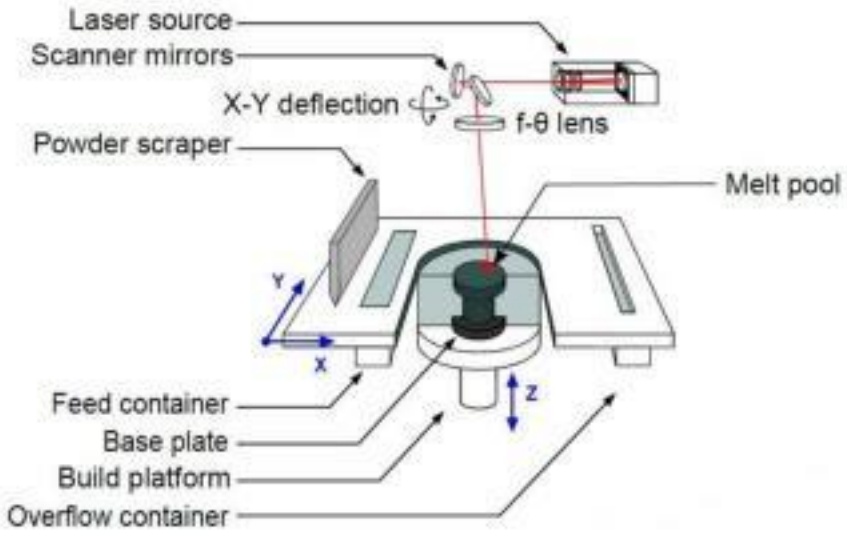

Figure 1.1 – SLM working schematic diagram

Generally speaking, spherical or near-spherical powder has good fluidity, it can be spread into thin layers, so as to improve the dimensional accuracy, surface quality, as well

as the density and organization uniformity of 3D printed parts. Therefore, it is the preferred shape type of raw material for 3D printing. However, it should be noted that the particle packing density of the ball powder is small and the gap is large, which makes the density of the parts small and also affects the forming quality. The development of metal powder preparation technology for 3D printing restricts the development of 3D printing metal parts industry. The breakthrough of low-cost preparation technology of metal powder for 3D printing has become an urgent problem for researchers at home and abroad. In recent years, domestic and foreign enterprises have invested a lot of capital and technical strength in the field of 3D printing metal powder preparation, and have made some progress. Figure 1.2 and Figure 1.3 show two kinds of metal powders.

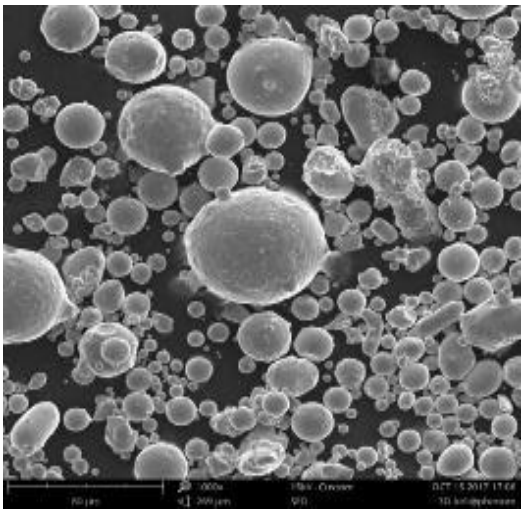

Figure 1.2 – Metal powder A

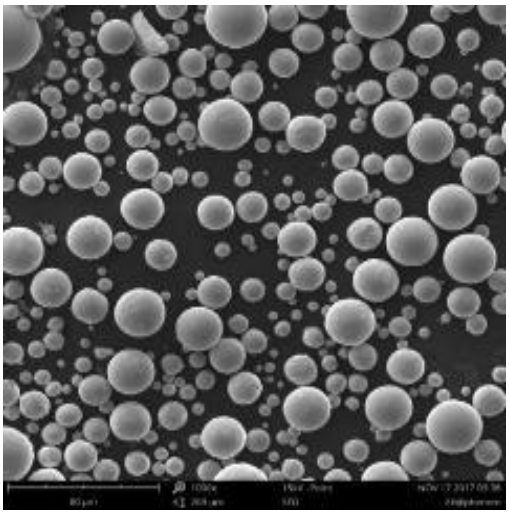

Figure 1.3 – Metal powder B

Figure 1.2 and Figure 1.3 are two kinds of metal powders. The comparison of the microscopic morphology of the two powders with feiner table scanning electron microscope shows that metal powder A is better than metal powder B. Metal powder A is basically A full ball of particles, almost no stick together.

Generally speaking, the smaller the particle size of the metal powder, the better the sintering process, because the smaller the particle size, the larger the specific surface area, the greater the driving force of sintering. In addition, the small gap between fine powder particles and the close connection between adjacent powder layers are conducive to improving the sintering densification and sintering intensity. Small particles of metal powder can also be filled into the gap of large particles, can improve the powder packing density, which is conducive to improve the surface quality and strength of printed metal parts. However, the finer the particles, the better. If there are too many fine particles, the phenomenon of "spheroidization" will easily appear in the sintering process, which will easily lead to uneven powder thickness. The so-called "spheroidization" phenomenon is a phenomenon that the shape of the molten metal surface changes to the surface of the sphere under the action of surface tension in order to minimize the free energy of the system formed between the molten metal surface and the surface of the surrounding medium. "Spheroidization" usually causes the metal powder to melt and not solidify to form

a continuous smooth pool, Various internal defects are shown in Figure 1.4.

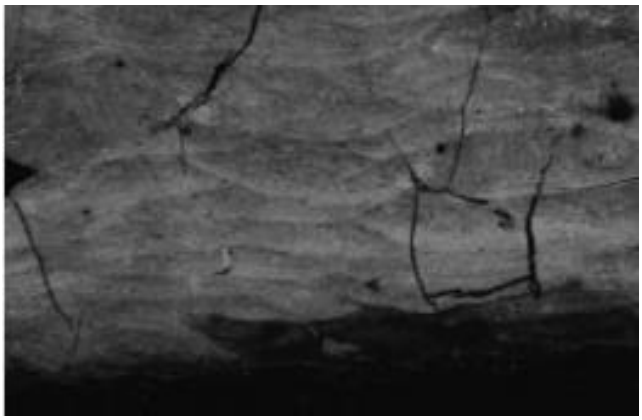

Figure 1.4 – Internal defects

Figure 1.4 shows the internal defect diagram of 3D printed parts of different granular metal. The particle size of metal powder used in 3D printing varies according to different heat sources. Generally speaking, the particle size of laser formed powder is between 30 m and 50 m, while that of electron beam formed powder is between 50 m and 90 m. The following is the use of feina desktop scanning electron microscope particle statistical analysis and measurement system for the detection of metal powder from a domestic manufacturer. The particle statistical system of SEM can not only obtain the results of roundness, length-to-length ratio, particle size and distribution of powder, but also obtain the morphology map of the detected area and the corresponding particle recognition status in real time. As can be seen from the particle recognition picture below, the particle statistical system is quite accurate for particle recognition, SEN scanning image and particle recognition image are shown in Figure 1.5 and Figure 1.6.

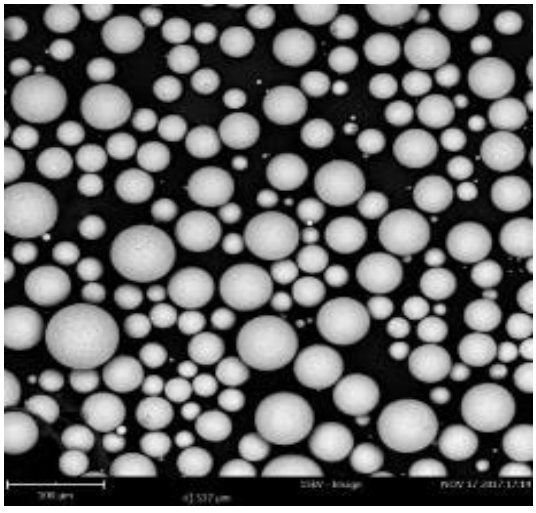

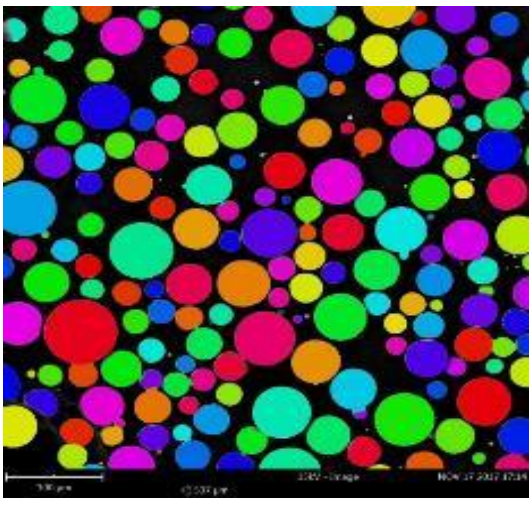

Figure 1.5 – SEM scanning image Figure 1.6 – Particle recognition picture

The particle size distribution curve of particle powder presents a gaussian distribution roughly, as shown in Figure 1.7

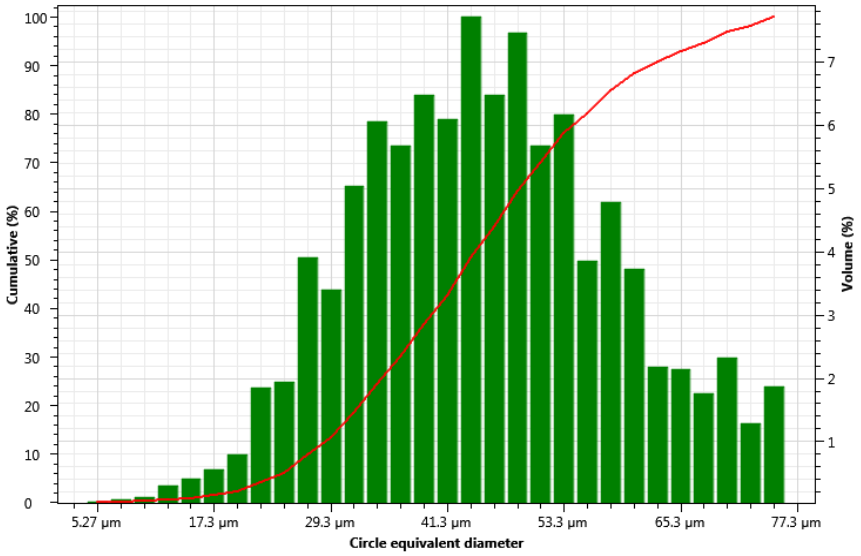

Figure 1.7 – Distribution of particle diameter

In the metal in the process of 3 D printing, in order to improve the density, the sphere of the metal powder particles, particle size, particle size distribution and so on all has certain requirements, to ensure that the qualification rate of products, at the same time, when the above factors is selected, if further optimization on the arrangement of particles, which can effectively improve the density in the process of the molten metal filling, and about the quality of the von berg system to make contribution to the improvement of mechanical properties, based on this, this paper focuses on different particle size distribution, particle size of the size of the particles in different containers to arrange physical properties.

1.5 Research content of the paper

This paper mainly focuses on the application and process analysis of metal powder 3D printing in turbine blade manufacturing. The purpose of this project is to study the density of metal powder particles in metal 3D printing, and to apply it to the field of metal 3D printing to improve the comprehensive performance of printed parts. Through physical experiment and numerical simulation, the density of spherical powder particles with normal particle size distribution was investigated. To be specific, the three-dimensional vibration test platform designed and manufactured by ourselves is used to carry out physical experiments on spherical metal particles with approximately normal particle size distribution, obtain the maximum density and record the optimal vibration parameters, and verify the experimental results repeatedly. By fitting the normal distribution function of particle size distribution of metal powder particles used in the physical experiment, an appropriate hard ball particle model was established, and the corresponding visualization results and dynamic characterization were obtained through the simulation of particle flow discrete element visualization programming software. Then the experimental results are compared with the numerical simulation results. In order to realize the high-density

accumulation of complex spherical powder particles with normal particle size distribution, the optimal parameters are obtained, which lays a foundation for further research on the density of spherical powder particles and guidance for industrial application.

This paper reasonably plans the design process according to gant's diagram, and analyzes the application and advantages and disadvantages of metal 3D printing technology in turbine blade manufacturing through SOWT, paving the way for future research.

2 EXPERIMENTAL EQUIPMENT AND MODELING

2.1 Establishment of experimental platform

To the description of the real results, you first need to various parameters affecting the metal powder particle density were analyzed, and the second, through independent design and manufacture of can realize three X, Y, Z axis perpendicular vibration test bench for physics experiment, the vibration test bench, on the basis of meeting the basic experimental requirement structure cooperate closely, simple manipulation, low cost, by adjusting the air switch, not only can realize the three directions of vibration at the same time, also can achieve any two direction of vibration at the same time, as well as any single direction of vibration. The safety of the experimenter can be guaranteed by controlling the main switch of power supply, frequency converter and air switch.

2.1.1 Motor selection

The basic principle of the test bench is as follows: the vibration force generated by the vibration motor is transmitted to the roof of the vibration table, and the vibration force and direction of the three-dimensional vibration table are adjusted by the vibration motors installed in three different directions, so that the vibration table can produce vibration in different directions.

Since the vibration process is reciprocating motion, ac servo motor is selected for the motor.

At the same time, the model of the motor is selected according to the size of the excitation force, vibration speed and torque required by the test bench, and the method for calculating the motor power and torque is as follows:

1. Motor power calculation method (2.1):

$$P = F \times V, \tag{2.1}$$

where P - motor power (KW),
F - motor force (N),
V - vibration speed.

2. Calculation method of motor torque (2.2):

$$T = 9550P / n, \tag{2.2}$$

where T - motor torque (Nm),
n - rated speed of the motor (r/min).

After calculation, the model of vibration motor in the vertical direction is YZD-5-4, and its rated power is 0.25KW.

The model of vibration motor in horizontal X and Y direction is YZD-1.5-2, and the rated power is 0.12kw. Considering that the three plates can vibrate independently and jointly.

2.1.2 Structural design

Based on considering stability, in the structure design, for the base of the test rig choose steel structure, guarantee the stability and smoothness of base, for the main part of the test bench, need to use 3 D modeling software for the whole simulation, first starting from the overall structure of three-dimensional vibration test rig for design and analysis, then the mechanical parts of the contact type between the choice of appropriate, and consider the machining precision of parts and materials selection, finally selected the size of various parts, and use the CAD machining of mechanical drawing software.

According to the size of the guide plate and the load borne by the slide rail, and considering the convenience of processing, the models of the four slide rails are based on the model on the x-direction guide plate, and the type of slide rail is SBR16U. The lower end of the spring is inserted into the vertical column of the base to ensure the safety of the spring link. The model number of the spring is chosen as 1060150 (mm) according to the size of the column on the base.

2.1.3 Strength and stiffness check

After the structural drawing was completed, the team performed a mechanical analysis of the columns on the roof for safety.

Because there is not a whole between the roof and the column, when the three-dimensional vibration table vibrates, there will be a dangerous section to destroy the structure at the welding place.

According to the vibration motor is a force object, vibration table is a force object. In the horizontal direction, the stress is mainly shear stress, and the stress concentration occurs in the welding of the upper roof and the vertical column.

At the same time, the vertical direction of the tensile stress. After checking, the shear stress is greater than the motor excitation force, the tensile stress is greater than the vertical direction of the excitation force, so the welding of the roof and column is safe.

1. method to judge the strength of parts

Determine whether the maximum stress at the risk section is less than or equal to the allowable stress. In this case, the strength condition can be written as (2.3) and (2.4):

$$\sigma \le [\sigma],\ \ [\sigma] = \frac{\sigma_{\lim}}{[S_\sigma]}\ , \qquad (2.3)$$

$$\tau \le [\tau],\ \ [\tau] = \frac{\tau_{\lim}}{[S_\tau]}\ , \qquad (2.4)$$

Judge whether the actual safety coefficient at the dangerous section is greater than or equal to the allowable safety coefficient.

In this case, the strength condition can be written (2.5) and (2.6):

$$S_\sigma = \frac{\sigma_{\lim}}{\sigma} \ge [S_\sigma]\,, \qquad (2.5)$$

$$S_\tau = \frac{\tau_{\lim}}{\tau} \geq [S_\tau], \qquad (2.6)$$

The method of calculation is usually determined by the available data and computing conventions.

2. static stress intensity

The strength failure of a part under static stress is characterized by plastic deformation or fracture.

For the plastic material parts under one-way stress, the strength is calculated under the condition that no plastic deformation occurs. Then, the limits in equations (2.3), (2.4), (2.5) and (2.6) should be the yield limit of the material, and the stress concentration is not considered in the calculation.

For plastic material parts under composite stress, the strength condition is determined according to the third or fourth strength theory. When bending and torsional composite stress is calculated with the third or fourth strength theory, the strength conditions are as following (2.7) and (2.8):

$$\sigma = \sqrt{\sigma_b^2 + 4\tau_T^2} \leq [\sigma] \ , \qquad (2.7)$$

$$\sigma = \sqrt{\sigma_b^2 + 3\tau_T^2} \leq [\sigma] \ , \qquad (2.8)$$

The approximate value is calculated according to the third strength theory, and the approximate value is calculated according to the fourth strength theory.

The formula for calculating the composite safety coefficient can be obtained as follows (2.9) and (2.10):

$$S = \frac{\sigma_s}{\sqrt{\sigma_b^2 + \left(\frac{\sigma_s}{\tau_s}\right)^2 \tau_t^2}} \leq [S], \qquad (2.9)$$

$$S = \frac{S_\sigma S_\tau}{\sqrt{S_\sigma^2 + S_\tau^2}} \leq [S] \ , \qquad (2.10)$$

For parts which allow a small amount of plastic deformation, the strength can be calculated according to the load allowed to reach a certain plastic deformation, the plastic deformation value is determined by the actual use.

When the cyclic characteristics are constant, the maximum stress of the material without fatigue failure becomes the fatigue limit after the stress cycles N times, and is denoted by.

When the above formula is used to calculate the fatigue strength, the ultimate stress is the fatigue limit. In addition to cycle characteristics and cycle times, there are also stress concentration, part size, surface state, etc., which affect the fatigue limit of parts. When these factors cannot be considered in detail, the method of reducing allowable stress or increasing allowable safety factor can be used for approximate calculation.

2.2 Experimental design

2.2.1 Experimental instrument design

The following Figure 2.1 and 2.2 shows the structure schematic diagram of the 3d shaking table：

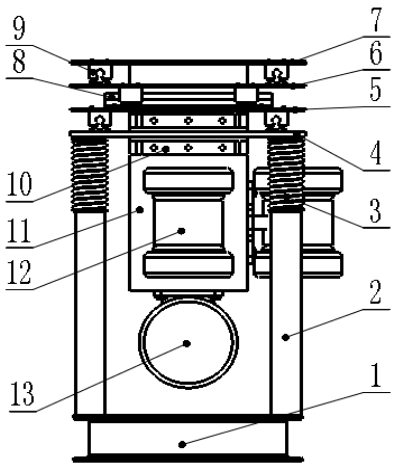

Figure 2.1 –3D shaking table　　Figure 2.2 –Experimental device

Experiment device of two-dimensional front view as shown in Figure 2.1, Other auxiliary devices and equipment include: frequency converters, air switches, plexiglass containers. The physical picture of the experimental device is shown in Figure 2.2. In the process of experiment, the amplitude is controlled by controlling the internal eccentric wheel of the vibration motor, and the vibration frequency is controlled by adjusting the frequency of the frequency converter. The vibration control equation in all directions is (2.11):

$$S = A\sin(2\pi ft + \phi) \ , \qquad (2.11)$$

where S - displacement, mm; A -- amplitude, mm; T - vibration time, s; Φ - in the early phase.

In the actual experimental process, the amplitude, vibration frequency and vibration time are the main experimental parameters, which directly affect the experimental density results of particle accumulation.

In this paper, the speed n of the vibrating motor is proportional to the frequency, and the relation is as follows (2.12):

$$\mathrm{n} = \frac{N_e f}{60 f_e} \ , \qquad (2.12)$$

where n - the actual speed of the motor, r/s;

N - rated speed of the motor, r/min;

N_e - actual output frequency of the motor, Hz;

f-- rated output frequency of the motor, Hz;

The technical parameters and ratings of the above vibrating motor are shown in table 2.1.

Table2.1 – Model and rating of vibration motor

Model	Rated excitation force, KN	Rated power, KW	Rated current, A	Rated speed, r/min	Rated frequency, Hz
YZD-1.5-2	1.5	0.12	0.36	3000	50
YZD-5-4	5	0.25	0.75	1500	50

In this paper, the vibration of motor selection for ac induction motor, the speed depends on the series and the output frequency of the motor, motor series. Therefore, in the process of experiment is difficult to control by adjusting the vibration motor series means speed, and the output of the motor frequency can be controlled by external frequency converter, therefore, the inverter is the key to the speed of vibration motor.

The related parameters of the inverter in this paper are shown in table 2.2:

Table2.2 – Model and rating of frequency converter

Model	Rated input voltage, V	Rated input current, A	Rated output, KW	Rated input frequency, Hz
SVF-MN1.5T4B	380	3.7	1.5	50

The experimental material used in this paper is iron powder with an average particle size of 0.3mm, and the experimental container is selected as plexiglass container, because it has many advantages such as easy to process, small error, easy to measure and observe, and small cost. A 300mm high container was used for the experiment.

2.2.2 Experimental flow design

By the content of the introduction, the powder particle density in the two dimensional vibration is higher than a single vibration condition, and the level of vertical direction to each other on the two-dimension vibration experiment, roughly selected each time about 30 s vibration experiment, at the same time, under the different amplitude by frequency

converter to adjust output frequency of the vibration motor, obtains the best experiment parameters matching, thus in the process, the level of the amplitude and frequency of the two directions are the same. The experiment adopts the method of integral feeding.

Before the experiment, firstly, adjust the position of the inner eccentric block in the 1.5-2 vibration motor and the 5-4 vibration motor to determine the amplitude of vibration, and then adjust the output frequency of the vibration motor with the frequency converter. Secondly, fix the container of the material to be vibrated, load the vibratory material, and measure the height of the material in the container. Finally, the vertical direction of each layer plate of the shaking table is aligned to ensure.

2.3 Mathematical model of particle accumulation

2.3.1 Particle accumulation parameters

The basic parameters to characterize the packing state of particles include porosity, packing density, coordination number, specific surface area and void distribution, among which porosity (or density) is the most widely used.

1. porosity (2.13):

$$P = V_q/V_a = (V_a - V_p)/V_a = (1 - \rho_a)/\rho_p \,, \qquad (2.13)$$

Where, V_q represents the volume of the void in the particle,V_a--the apparent volume of the particle, V_p--the true volume of the particle, ρ_a--the apparent density of the particle, and ρ_p--the true density of the particle.

2. packing density (2.14)

The bulk density is defined as the volume ratio of solid particles in the particle body (2.14):

$$D = 1 - P = \rho_a/\rho_p \,, \qquad (2.14)$$

3. coordination number

The coordination number is defined as the number of contact points of each particle and other surrounding particles, which is related to the rheological property of the particle body.

4. apparent density

Apparent density is the ratio of particle mass to particle volume. It can be seen from the above that the relationship between apparent density, true density and void fraction of the accumulation body is as follows (2.15):

$$\rho_a = (1 - \varepsilon)\rho_p \,, \qquad (2.15)$$

5. particle size dispersion

For the particle size distribution, it is often necessary to measure the particle size distribution, and the particle number distribution and mass distribution are often used to define the particle dispersion. Dispersion is the proportion of the number of particles (mass or surface area) in some particles with different size ranges.

6. particle size distribution function

Particle size distribution can be expressed in tables and graphs, but it is more convenient to express it in a functional form for mathematical analysis.

Particle size distribution function is a mathematical expression of the relationship between particle size distribution and particle size.

2.3.2 Equal diameter ball stacking model

For the regular filling of a sphere, its density is closely related to the arrangement of the sphere, as shown in the below Figure 2.3 and Figure 2.4.

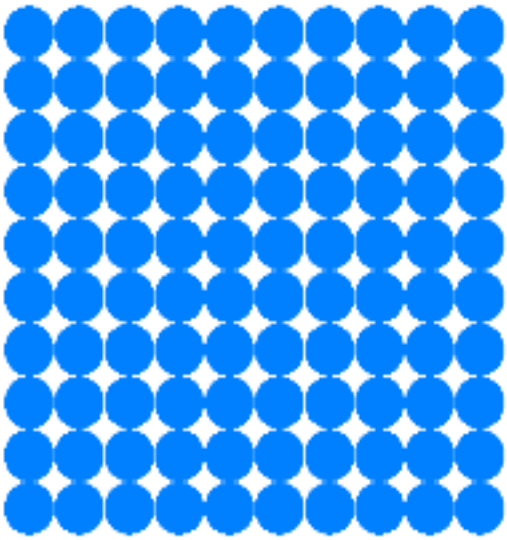

Figure 2.3 – Simple cubic stacking

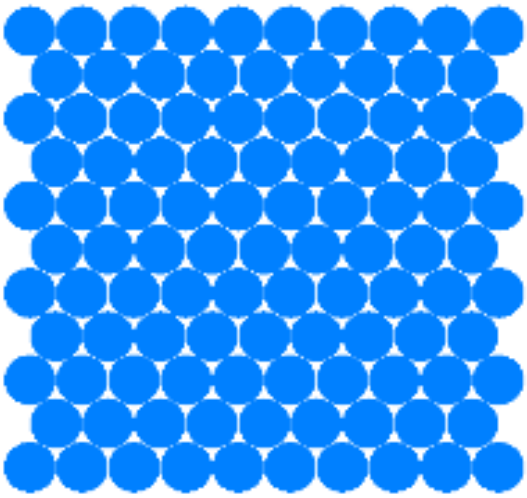

Figure 2.4 – Hexahedral stacking

The numerical equation for calculating the accumulation density of particles under the arrangement law shown in Figure 2.16 and Figure 2.17:

$$\lambda_1 = 1 - {4/3\pi R^3}\Big/{(2R)^3} = 1-{\pi}/{6} \approx 0.4764 \quad , \qquad (2.16)$$

$$\lambda_2 = 1 - {8\pi R^3}\Big/{\left(6\sqrt{3}R^2\right)\left(4R\sqrt{{2}/{3}}\right)} = 1-{\pi}/{3\sqrt{2}} \approx 0.2595 \, , \qquad (2.17)$$

Through the establishment of the above ideal model and the derivation of the mathematical formula, the corresponding relation between the arrangement pattern.

The density of the isopod sphere can be obtained as shown in table 2.3.

Table 2.3– Density distribution parameters of isopod sphere with different arrangement

Arrangement	Coordination number, N_c	Density, D%	Porosity, P%
Cubic type	6	$\pi/6$	47.64
Six square	8	$\pi/3\sqrt{3}$	39.55
Compound hexagon	10	$2\pi/9$	30.19
Pyramid type	12	$\pi/3\sqrt{2}$	25.94
Hexahedron type	12	$\pi/3\sqrt{2}$	25.94

However, in practical production practice, the preparation and application of isopod spheres are relatively rare, and their arrangement only theoretically meets the parameters in the table above, while the actual arrangement of particles is relatively random, which makes it difficult to reach the theoretical density parameter value.

2.3.3 Grading the ball stacking model

1. Horsfield compacting theory

In the most densely packed arrangement of the angular cone or hexahedron, the gaps can be further filled according to the way of particle grading. A mathematical model is established according to the geometric relationship between the spheres. The arrangement of "rhombohedral shape" is obtained, and the so-called most dense accumulation -- Horsfield dense accumulation. The relationship between the number of gradations and the stacking density is shown in table 2.4.

Table 2.4 – Horsfield compacting model

series	The ball diameter, mm	Porosity, P%	Density, D%
Level 1 ball	R1	25.94	74.06
Level 2 ball	0.414R1	20.7	79.3
Level 3 ball	0.225R1	19.0	81.0
Level 4 ball	0.177R1	15.8	84.2
Level 5 ball	0.116R1	14.9	85.1
……	tiny	3.9	96.1

2. Interval stacking theory

The separation stacking theory, also known as Zhang Rongzeng's theory, is based on the premise that the ratio of the natural stacking particle size D to its void size is equal to the sieve ratio B, so the material is divided into several grades according to the sieve ratio B. It is assumed that in continuously distributed materials, if the volume of all particles in grade I +1 is smaller than the volume of the gap in grade I, and if the volume of particles in grade I +2 is exactly equal to the volume of the gap in grade I, the particle size composition can reach the maximum density accumulation (2.18):

$$\mathrm{n} = \ln^{1/\varepsilon} / \ln \mathrm{B}\,, \qquad (2.18)$$

Where, n represents the modulus of Gaudin and Alfred equations, represents the porosity of particles, and B represents the sieve ratio.

By computer simulation, when the modulus n of the above equation is 0.37, the material has the most compact accumulation.

3. Alfred compacting equation (2.19):

$$\mathrm{U}(D) = \frac{D^{N}_{n} - D^{n}_{min}}{D^{n}_{max} - D^{n}_{min}} \times 100\%\ , \qquad (2.19)$$

Where, U represents the content less than particle size D, D_{max} represents the maximum particle size,D_{min} represents the minimum particle size, and n represents the modulus.

2.3.4 Sphere accumulation model

Is common in nature, the normal distribution, and for metal field of 3 D printing, metal powder particles by reduction method, the atomization method, electrolytic process, mechanical Fen Suifa, hydroxyl method, direct method such as legal, among them, the method, electrolytic process and atomization method to produce powder as raw materials used in powder metallurgy industry is relatively common. The generated powder particles are micron in size, the sphericity requirements are high, and the particle size distribution tends to be generally normal.

The normal distribution function of particle (2.20 – 2.22):

$$\mathrm{P}(d_p) = \frac{1}{\sigma\sqrt{2\pi}} \times exp\left[-\frac{\left(d_p - \overline{d_P}\right)^2}{2\sigma^2}\right], \qquad (2.20)$$

$$\sigma = \left[\frac{\sum n_i \times \left(d_{p_i} - \overline{d_P}\right)^2}{N-1}\right]^{1/2}, \qquad (2.21)$$

$$\overline{d_P} = \overline{d_L} = d_{50} = d_d \ , \qquad (2.22)$$

Where, $\overline{d_L}$ is the arithmetic average diameter, and is the ratio of the sum of the diameters of all particles to the total number of particles; d_{50} Is the median diameter, and is the particle size whose cumulative frequency of particle size distribution is equal to 50%.d_d is the mass diameter, and is the particle size corresponding to the maximum probability density P value in the frequency density distribution curve.

In production practice, the particle size of the powder particles generated in many cases is asymmetrically normal. The particle size coordinates are replaced by logarithmic coordinates, and the distribution is approximate to the symmetric curve of normal distribution. It is said that the particle size conforms to the logarithmic normal distribution, and its functional form is as follows (2.23):

$$\mathrm{q}(d_p) = \frac{1}{\sqrt{2\pi}\times \ln \sigma_g} \times exp\left[-\frac{(\ln d_p - \ln d_g)^2}{2(\ln \sigma_g)^2}\right], \qquad (2.23)$$

Where,σ_g and d_g is the two characteristic Numbers of lognormal distribution,d_g is the geometric mean diameter ($d_g = d_{50}$), and σ_g is the geometric standard deviation (2.24):

$$\ln \sigma_g = \left[\frac{\sum n_i \times (\ln d_{p_i} - \ln d_g)^2}{N-1}\right]^2 , \qquad (2.24)$$

Because the number of particles generally greatly, therefore the particle size distribution of particle group is near to a smooth curve, size deviation phenomenon is not obvious, and second, in the process of particulate matter of actual settlement, because small particles to suspended or collision phenomenon, larger particles are so quick coagulation downward trend, further balance the settlement after the inner particle distribution of particulate matter. Therefore, the bulk density of particles with normal particle size distribution was studied in this paper.

2.4 Summary of this chapter

Aiming at the problem of part compactness in 3D printing of metal materials, it is proposed that spherical particles with normal particle size distribution are adopted in the metal printing stage, and the homogeneous density accumulation of multi-metal powder particles is realized by increasing the vibration function unit, and then the powder is spread, so as to improve the density. For this purpose, the 3d modeling software was used to design and the 3d vibration test bench was commissioned to manufacture. In order to improve the packing density of particles in the sphere, the effects of parameters such as particle distribution state, vibration amplitude and frequency.

In this chapter, the selection design, structure design, stiffness and strength check of the 3d vibration test bench used in the experiment are described in detail to ensure the

rationality of the design of the physical test bench and reduce the manufacturing cost as far as possible. Then, the accumulation model of spherical particles is described, and the theoretical accumulation density value under different particle accumulation is analyzed, which lays a foundation for future experiments and data checking. Finally, the mathematical modeling of the stacking parameters and the ball stacking model provides a theoretical basis for the numerical simulation. By comparing various stacking theories, the suitable particle model is obtained for the numerical simulation.

3 NUMERICLE SIMULATION

3.1 Simulation flow chart

Figure 3.1 is a numerical simulation flow chart.

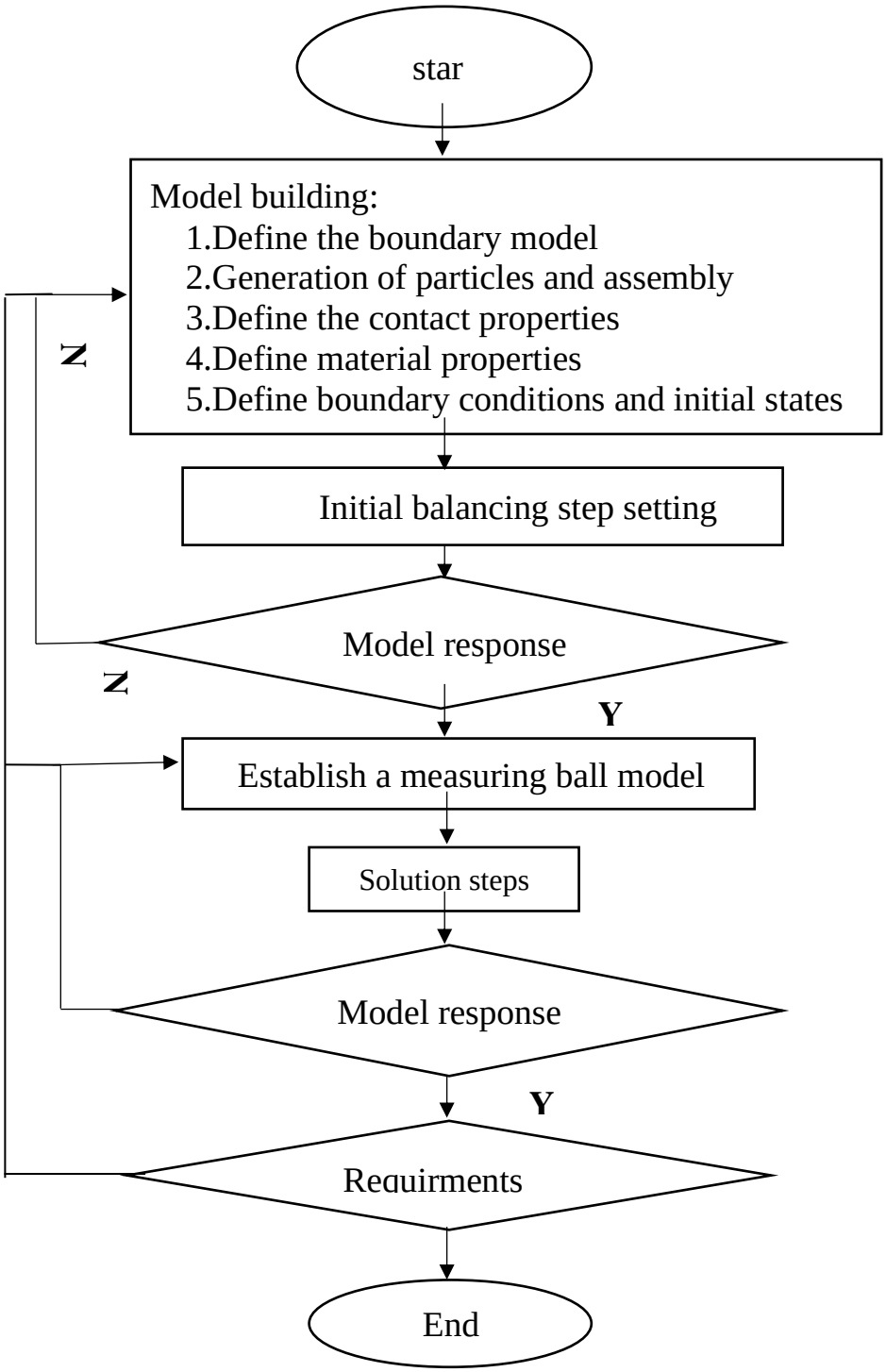

Figure 3.1 – Numerical simulation flow chart

The flowchart Figure 3.1 summarizes the operation of the whole numerical simulation and simulation stage, and carries out real-time monitoring and feedback on the model response and simulation parameters to ensure the rationality of the obtained data.

3.2 Simulation study on the stiffness coefficient

3.2.1 Initial condition setting

The particle size of 0.3mm was simulated, and different stiffness coefficients were set respectively. Other relevant influencing factors and variables were set as follows:

1. Cylindrical boundary container is adopted, and the ratio between the diameter of the container and the diameter of the ball is adopted to eliminate the influence of boundary size as much as possible.
2. The measuring ball used to measure the particle density inside the container should be kept at a certain distance from the container wall, so as to eliminate the influence of the surrounding walls on the particle density inside the container as far as possible.
3. Adopt the method of overall feeding, and set the connection model between the spheres and the connection model between the spheres and the wall as the linear elastic model.
4. The normal and tangential stiffness of the sphere and the sphere and the wall are equal to each other.
5. The friction coefficient between the spheres is 0.015, the damping ratio is 0.2, and the sphere density is set to 7800kg/ m^2.
6. A measuring ball with a radius smaller than the inner diameter of the charging barrel is set at the outlet of the charging funnel, and the same measuring ball is set at the top and bottom of the charging barrel for numerical simulation.
7. The number of random seeds was set to be large enough to ensure the consistent distribution of particles in each verification experiment. In this paper, the number of random seeds was 10001.

3.2.2 Model establishment

The discrete element program command software is used to simulate and analyze the process of numerical simulation and simulation. The model properties are set according to the above parameters, and the simulation process is designed according to the flow chart.

The following is the visual interface of the simulation process.The diameter of the barrel is 10mm and the diameter of the measuring ball is 8mm. The distribution of the measuring ball in the particle accumulation body is shown in the Figure Different colors represent the position of the measuring ball center. The vertical coordinate of the blue measuring ball is -7mm, the vertical coordinate of the green measuring ball is -16mm, and the vertical coordinate of the bottom measuring ball is -25mm.

As shown in Figure 3.2, the number of generated particles is 13,792, and the particle size is set as a sphere of equal diameter of 0.3mm.

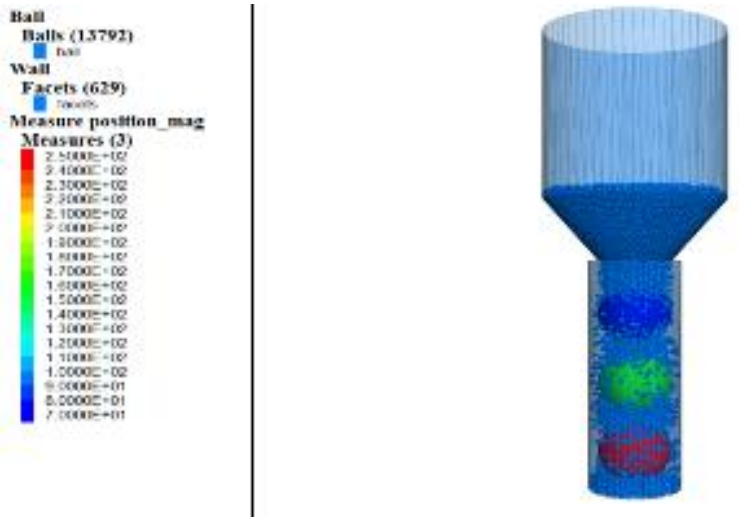

Figure 3.2 – Packing and porosity measurement ball setting

As show in Figure 3.2, All models are located in the solution domain.

3.2.3 Numerical simulation

The establishment of the model is the foundation of solving the model, and the numerical simulation is the core of solving the model.

For the particle body, when the initial conditions are determined, the initial model of each simulation can be kept consistent by setting random seeds, and the particle size distribution and relative position of the generated particle body can be kept unchanged, which is conducive to the repetitive simulation and simulation of the model by using the control variable method. As shown in Figure 3.3 is accumulation between internal sphere particles stress gram and stress distribution.

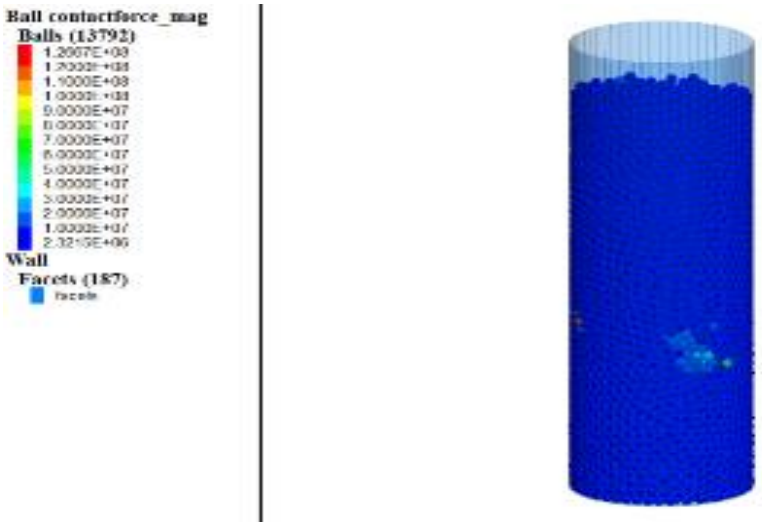

Figure 3.3 – Schematic diagram of the stress cloud diagram between particles in an equal-diameter packing sphere

Computation will focus on some of the local area or a sphere, resulting in local result shows error, this paper simulated particle number is 13792, but appear error on the number of particles is about 20, the error rate of only about 1.45 ‰, it can be neglected, a single particle of iterative computation error will cause the overall local produce large amount of calculation is not balanced. As shown in Figure. 3.4 schematic diagram of velocity cloud diagram between particles in packing balls of equal diameter.

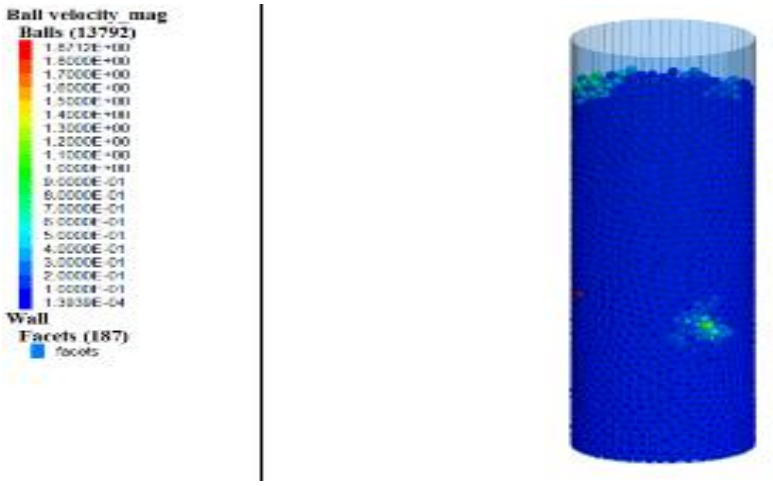

Figure 3.4– Schematic diagram of the velocity cloud diagram

By comparing the cloud map corresponding to Figure 3.3 and Figure 3.4, it can be found that the distribution law of the two is very similar, because the numerical simulation adopts the basic mechanical operation model, and the force and velocity are the basic physical quantities to describe the dynamics, and there is a strong correlation between them. As show in Figure. 3.5 is the spherical displacement cloud image. As shown in Figure 3.6 is the cloud image of the position of the sphere.

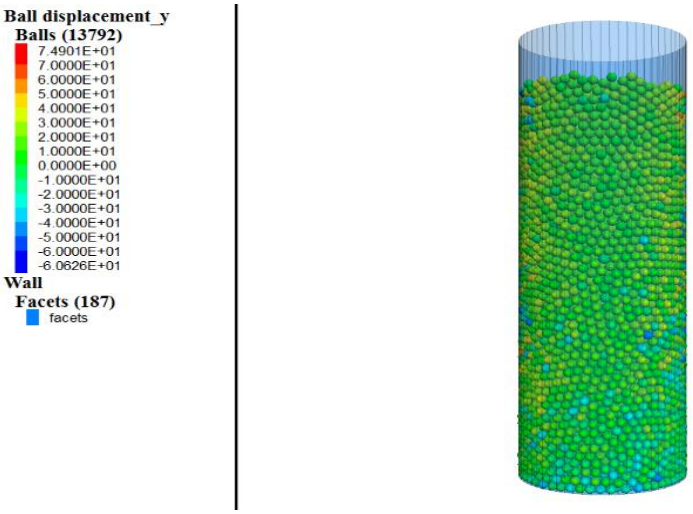

Figure 3.5 – Cloud image of sphere displacement

Deposit as shown in Figure 3.5 for the internal particle displacement gram, the distribution of basic proportional to the vertical coordinate, displacement boundary is not obvious, but there are mutual crisscross zone of transition, demonstrating that particles in layered accumulation at the same time, the internal particle relative to rub together, will happen because of the random collision and friction between particles, leading to the same initial height of particles body no longer maintain the same level in the process of accumulation. As shown in Figure 3.6 is cloud image of sphere position.

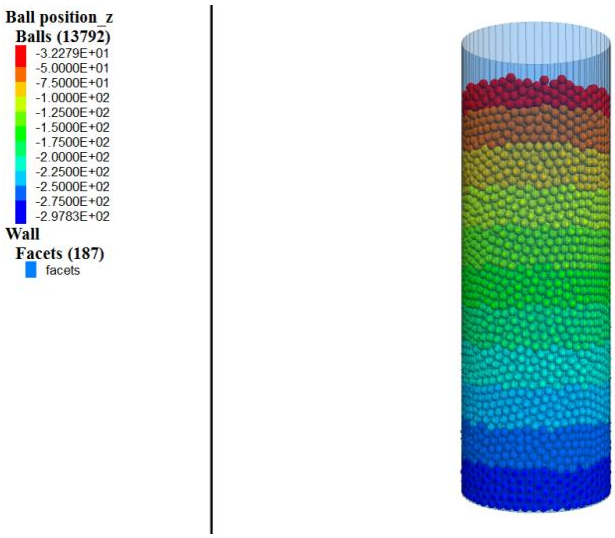

Figure 3.6 – Cloud image of sphere position

Figure 3.6 shows the particles between the schematic diagram of the x-axial displacement and the position cloud map in an equal-diameter. Displacement for different particle size affect the position and the distribution of stress, for a single particle contact point of the dependent variable corresponding effects, for the deposit, the accumulation of general rule is not affected. As shown in Figure 3.7 is the schematic diagram of the particles in the y-axial displacement and position in an equal-diameter packaging field.

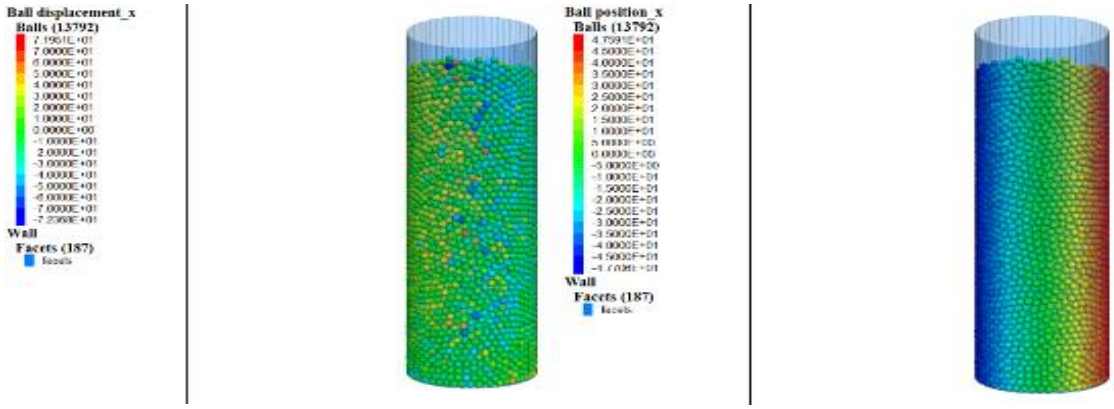

a X-axis displacement b X-axis position

Figure 3.7– Schematic diagram of the X axial displacement and position

Figure 3.7 shows the distribution, most of particle displacement is less than 4 mm. There are some particles in the process of falling due to collision, from one end of the container wall movement to the other end, the displacement could reach 8 mm. As shown in Figure 3.8 is schematic diagram of y-axial displacement and position among particles in an equal-diameter packing sphere.

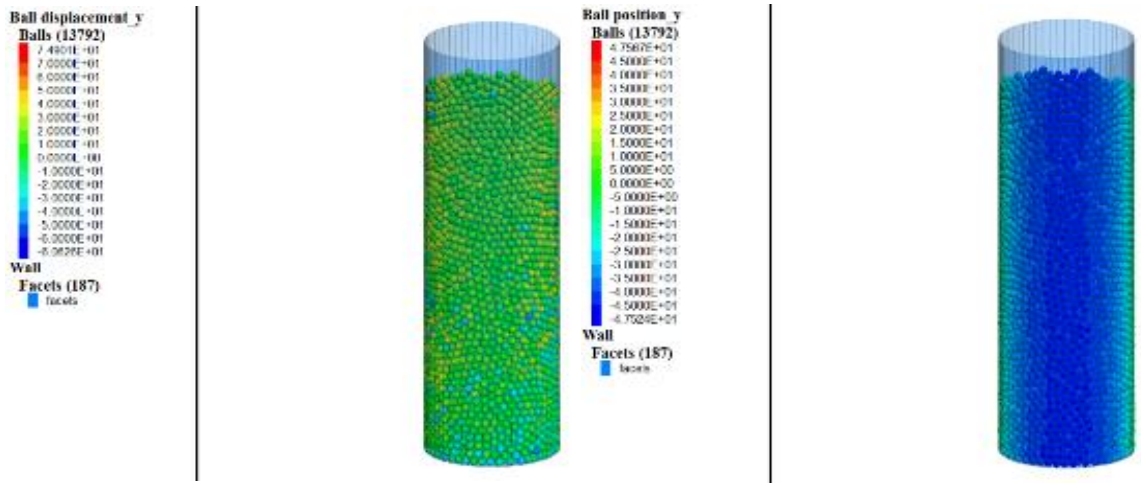

a Y axial displacement b Y axial position

Figure 3.8 – Schematic diagram of Y-axial displacement and position

Figure 3.8 can be regarded as the front view and side view of the radial distribution of the spherical position cloud image. The two images are very similar, mainly because the container is a cylinder. As shown in Figure. 3.9 shows Z axis displacement and position of particles in packing balls of equal diameter.

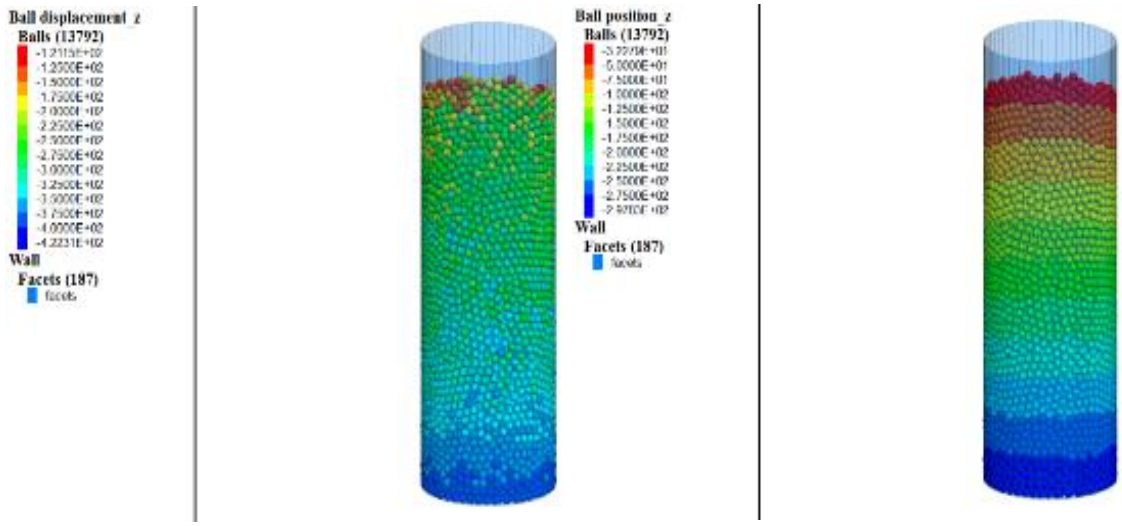

a Z-axial displacement cloud b Z-axial position coordinate cloud

Figure 3.9 – Schematic diagram of Z-axial displacement and position

Since the origin coordinate of z-axis is located at the center of the top surface of the cylinder container, each value represents a negative value. In addition, the distribution in Figure 3.9 is basically consistent with that in Figure 3.5, because the movement of particles in the horizontal direction has little influence on the displacement and coordinate change in the vertical direction.

By stacking sphere contact stress gram position and velocity contours, displacement gram and cloud, can be in the process of sphere accumulation intergranular stress and accumulation structure have more accurate understanding and analysis to the accumulation of particles body internal laws, and the actual accumulation process were analyzed, thus to adjust the parameters of the initial value, optimize accumulation model and the numerical simulation process, it is concluded that more accurate simulation.

For the measurement of particle porosity, the porosity measurement ball model is mainly established and activated in the process of numerical simulation to realize the real-time monitoring of the porosity inside the accumulation body.

3.2.4 Measurement of porosity

As shown in Figure. 3.10 variation curves of porosity of the sphere obtained from different measurements.

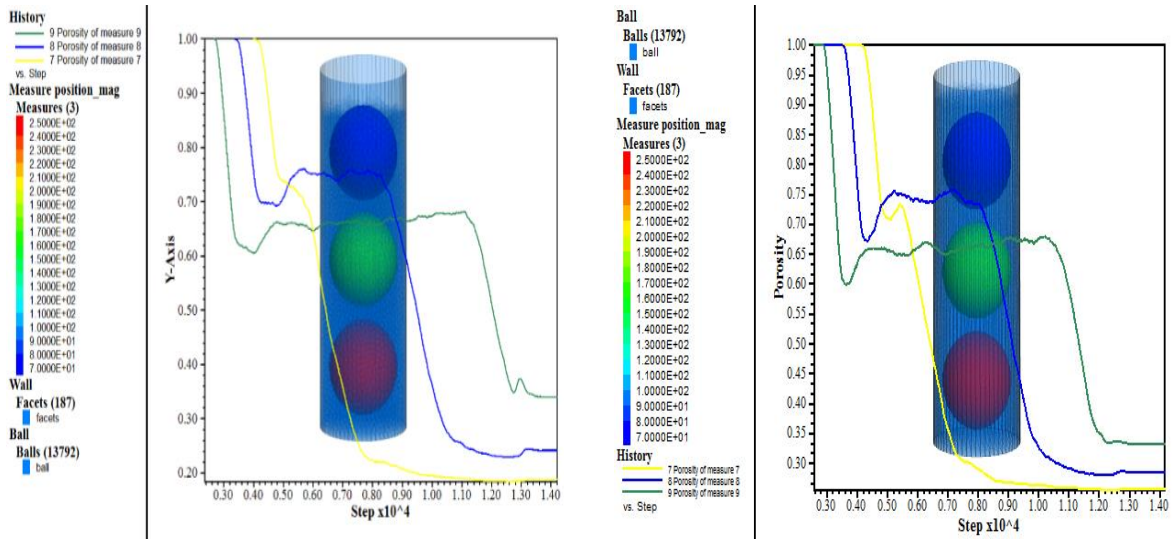

Figure 3.10 – Variation curves of porosity of different measured spheres

Figure 3.10 shows the variation curves of porosity of different measured spheres. The color of the measured ball represents the vertical coordinate value of each ball center when the center of the top surface of the container is zero. Yellow curve P7, blue curve P8, and green curve P9 respectively represent the data curve of the ball measured from the vertical position from bottom to top. There is a certain time difference in the data collection of the porosity measurement curve, because in the falling process of the sphere particles, they pass through blue, green and red measurement balls in turn, and the red measurement balls are the first to be filled.

In the initial stage of each curve, the porosity changes rapidly, because the sphere can be filled with a larger space range as soon as it enters the measuring sphere. Over time, each measuring ball measured porosity is stable for a period of twists and turns, this is because in the movement of the ball will be preferred filling material barrel bottom, and other highly particle movement and particle distribution of basic remains the same, and measure the ball from top to bottom in turn smooth twists and turns of time shortened, blue measuring ball was finally filled, consistent with the actual.

The interval time from the initial state to the steady state of the porosity curve of P7, P8 and P9 gradually increases, which also indicates that the filling order of the particle accumulation process is from bottom to top. At the same time, the obtained stable value of porosity gradually increases, indicating that when K=1e9.

The reason lies in the rigidity properties of granular material itself, because the stiffness of the smaller sphere particles exist large amount of overlap at contact, have a great effect on the reduced porosity, and the cylinder bottom particles in addition to the contact force between each other, also from upper particles under gravity, amount of overlap at the contact point sphere particles upper-layer particles is bigger, the space between the particles is compressed, the resulting particles lower body particles porosity is lower than the upper body.

The results show that the particle stiffness coefficient has a direct effect on the packing density of iso-diameter spherical particles. In order to explore the influence of stiffness on the packing density, an iso-diameter spherical particle body with particle size of 0.3mm was set. The control variable method was used to change the stiffness value K of the generated particle body on the premise of keeping other parameters unchanged. The simulation was carried out according to the simulation process described above to obtain the corresponding porosity.

3.2.5 Results analysis

For the same measurement ball, the porosity of the spherical particle accumulation gradually increases with the increase of the sphere stiffness, and finally approaches to the constant value of 0.37. The numerical simulation results show that when the ball stiffness reaches above 5e9, the porosity of the iso-diameter ball inside the barrel is 0.37 and the packing density is 0.63.

The numerical simulation results in this paper are consistent with the physical experiment results conducted by Scott, which indicates the rationality and feasibility of the numerical simulation and simulation model in this paper. When the particle distribution must be on the same stiffness under different porosity curve were analyzed, the results show that with the increase of pile depth, porosity of sphere particles gradually reduce the trend, but when the stiffness value reaches a certain value, stack depth basic had no effect on the sphere particles porosity.

For different stiffness under different porosity curve were analyzed, the results show that with the increase of stiffness sphere particles, the depth of different pile porosity difference gradually narrowed, eventually when the stiffness value reaches a certain value,

the depth of different pile porosity difference value is 0, particle packing density is uniform distribution status.

3.2.6 Failure analysis of stiffness parameters

By the results of the numerical modeling and simulation with Scott did physical, comparing the experimental results prove that the diameter of rigid sphere in rigid containers such as a maximum of random packing density is about 0.63, and with the increasing stiffness value of sphere, and by the simulated data available, spherical porosity in 0.37 and no longer changes, the amount of overlap between the sphere contact almost to zero. According to the numerical simulation and simulation results, within the range of ball stiffness from 5e8 to 9e10, the porosity decreases with the increase of ball stiffness, and the accumulation density does not change when the stiffness of ball exceeds 9e10. Next, the variation of the packing density of the sphere is discussed when the stiffness of the sphere is less than 5e8. When K=1e8, although the number of particles is basically the same as that simulated for K, the accumulative particles fail to cover all the measured balls, and the initial judgment is that there is a large amount of overlap between the particles in contact with each other. It indicates that the particle accumulation density at the bottom of the barrel has reached 0.968, but the particle accumulation density at the top is 0, indicating that there is no sphere. When K=1e8, the overlap of the spheres at the bottom of the feeding barrel is relatively serious. As the vertical depth of the spheres in the feeding barrel increases, the overlap between the spheres gradually increases.

As shown in Figure. 3.11 is a schematic diagram of stacking balls at the bottom of feed barrel K=1e8.

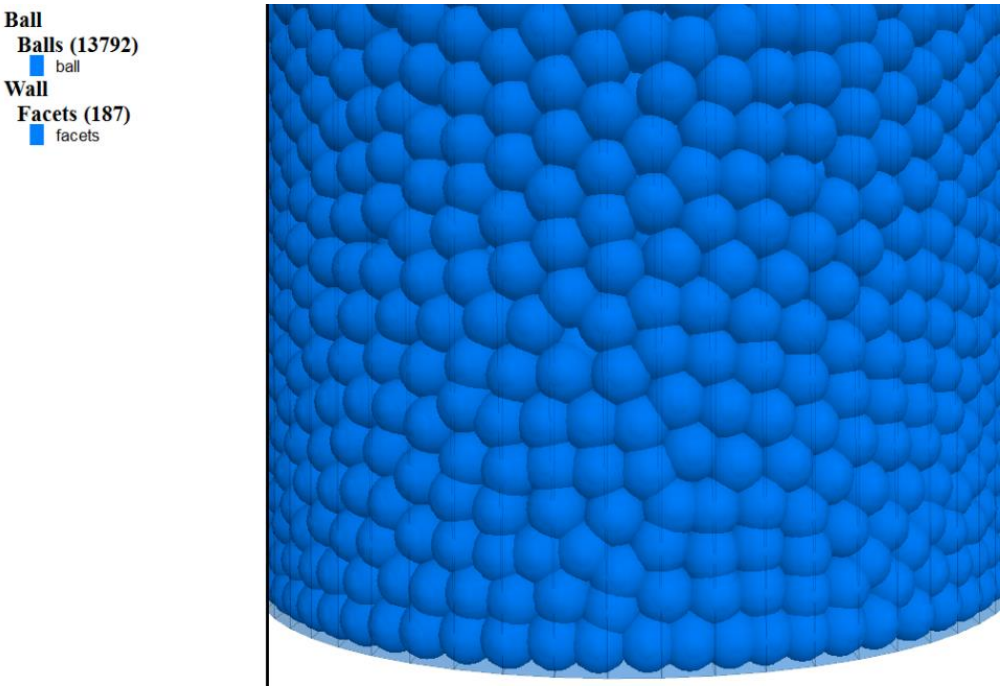

Figure 3.11 – K=1e8 view of ball stacking at the bottom of feed barrel

As the figure 3.11, Appear this situation because the grain density of 7800 kg/set, when the low stiffness of the sphere itself, particle body internal contact force and the gravity of the upper particle interaction, make the internal mutual contact between particles produces large elastic deformation, the final performance for the magnitude of the overlap between particles is larger, and the coincidence phenomenon is more obvious. Therefore, the particle density value set in this paper is not suitable for studying the packing density of particle materials of K5e8. To continue the research, a smaller particle density parameter value should be selected.

3.3 Numerical simulation of ball packing porosity

3.3.1 Initial condition setting

The simulated particle size mean =0.3, the spherical particle model with variance, the relevant influencing factors and variables are set as follows:

1. Cylindrical boundary containers were adopted, and the inner diameter of the container was proportional to the diameter of the ball, so as to eliminate the influence of boundary size effect on particle accumulation as much as possible.

2. The measuring ball used to measure the particle density inside the container should be kept at a certain distance from the wall of the container, so as to eliminate the influence of the surrounding walls on the particle accumulation density inside the container as much as possible.

3. Adopt the method of overall feeding, and set the connection model between the sphere and the sphere and the connection model between the sphere and the wall as the linear elastic model.

4. The normal and tangential stiffness of the sphere and the sphere and the wall are equal to each other.

5. The friction coefficient between the spheres is 0.015, the damping ratio is 0.2, and the sphere density is set to 7800kg/ m^2.

6. A measuring ball with a radius smaller than the inner diameter of the charging barrel is set at the outlet of the charging funnel, and the same measuring ball is set at the top and the bottom of the charging barrel for numerical simulation and software simulation.

3.3.2 Simulation and simulation

Packing container and 3 D model of porosity measuring ball, packing containers are 30 mm deep, measure the balls of different colors on behalf of the vertical coordinates of measuring the cue ball, accumulated in the center of container end face as the origin of coordinates, dark blue, light blue, green, red, four vertical coordinates of measuring the ball is in turn 4, 7, 16, 25, is an unit with mm. As shown in Figure 3.12 shows a container that generates a porosity measurement ball.

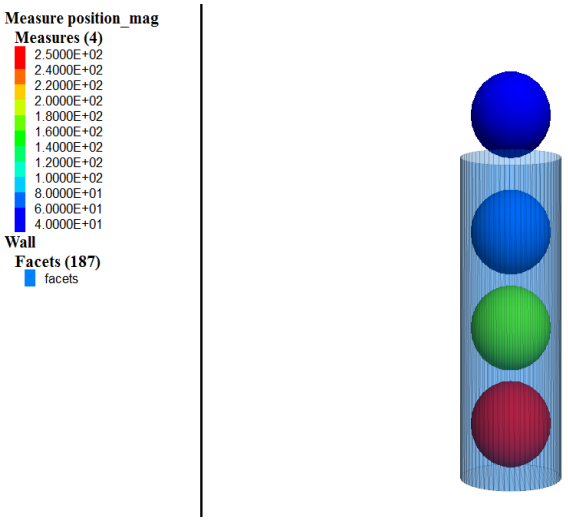

Figure 3.12 – A container with a porosity measurement sphere

In Figure 3.12 shows that during the natural sedimentation process of particles, the measurement ball performs real-time monitoring on the porosity of particles in the accumulation container. As show in Figure 3.13 shows particle modeling and solusion.

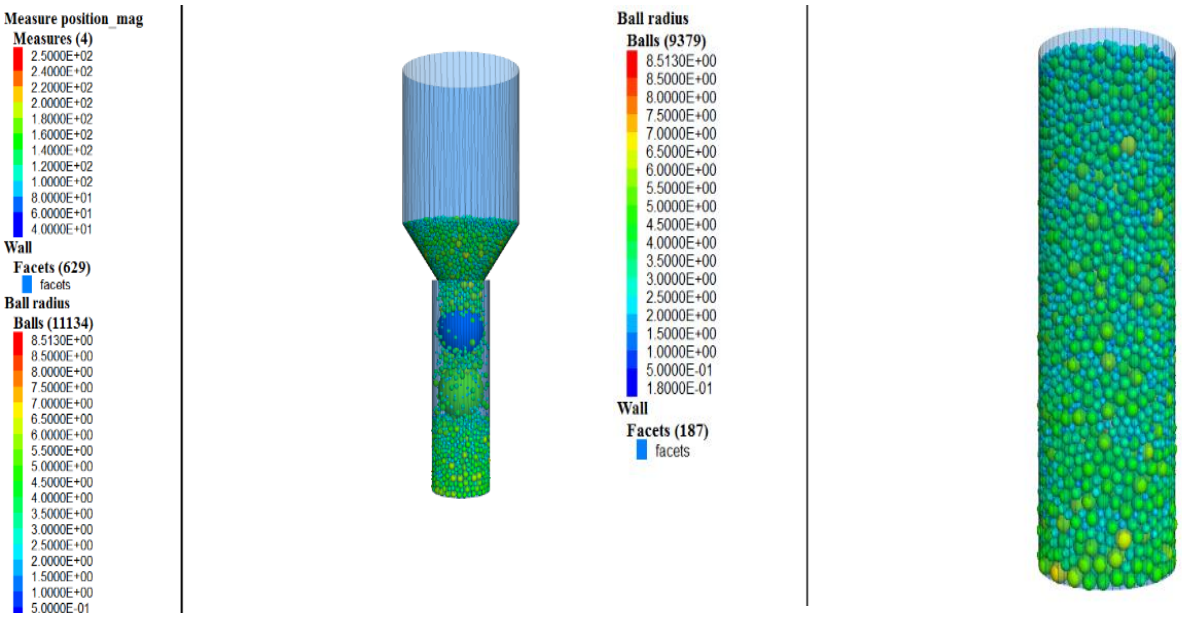

a Real-time monitoring b Completion of particle accumulation

Figure 3.13 – Particle modeling and solution

Figure 3.13 simulates the distribution state of particles after the completion of particle accumulation. The different colors of the particles in the Figure represent the size of particle size. It can be concluded that the particle size of the sphere is not different from each other. The particles of different sizes of the sphere are distributed in phases. However, for

the spherical accumulation model with normal particle size distribution, the particle distribution has a large randomness, so it is difficult to ensure that the accumulation porosity is the same everywhere. Therefore, necessary attention should be paid in the process of measurement and analysis.

3.3.3 Data analysis

As shown in Figure 3.14 shows cloud map of particle accumulation displacement.

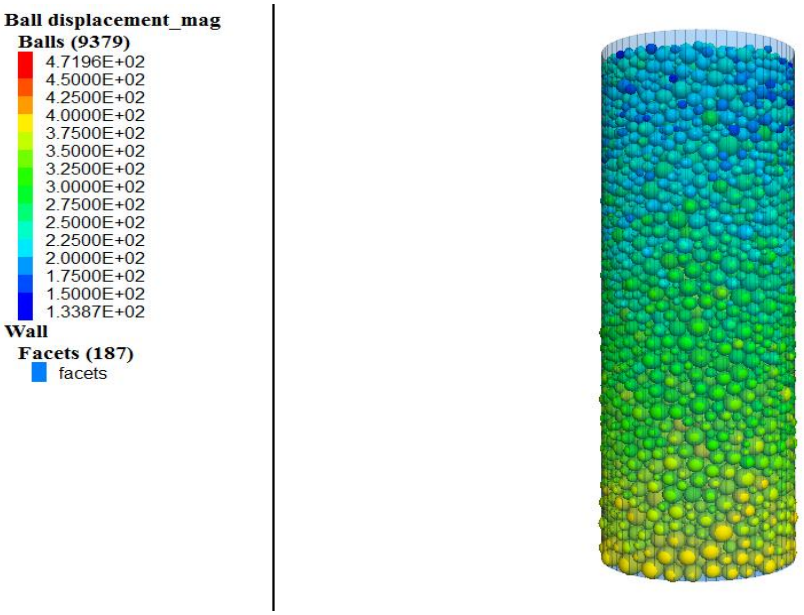

Figure 3.14 – Cloud image of particle accumulation displacement

As shown in Figure 3.14, represents the displacement cloud map of the movement of particles after the completion of stacking. The displacement of particles at the same height in the stacking container is not the same, but it generally shows a trend of increasing successively with the increase of the stacking depth.

In the same horizontal plane, the displacement of particles located near the central axis of the stacking container is greater than that of the particles distributed in the periphery, indicating that the particles at the flow center have a greater impact force during the stacking process, thus producing a relatively larger displacement. The porosity variation curves of the porosity measurement balls at K=1e9 in the middle and lower layers, middle layers and upper layers of the accumulation container are given below.

Curve of the initial porosity change quickly, because the initial into the sphere measuring ball can realize a bigger space range of filling, as time goes on, the measurement of the ball of the measured porosity will exist for a period of steady wave phase, this is because in the movement of the ball will fill the container bottom, first container upper maintain particles falling state of particle distribution, the accumulation of layered filling mechanism makes each measuring ball there are varying degrees of pseudo filling state, namely porosity stationary wave phase.

The method of control variables was used to change the stiffness value of the generated particles on the premise of keeping other parameters unchanged, and the stacking process of the spherical particles with normal particle size distribution was simulated. The change curve of the porosity of each ball was measured when the particles had different stiffness values K. with the sphere particles stiffness value increases, the porosity of the grain accumulation rate is roughly the trend of increase gradually, when the stiffness value, growth faster, leveled off after when the stiffness value. According to the Figure, when the stiffness value, there is a large amount of overlap between the particles in contact.

3.4 Study on the influence of different container sizes

3.4.1 Sphere model

1. equal diameter sphere model (r=0.3mm) (Figure 3.15)

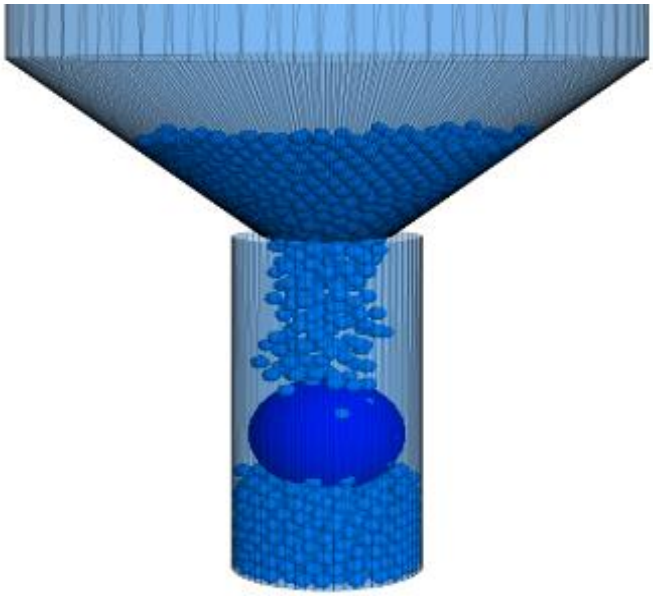

Figure 3.15 – Equal diameter sphere stacking model

As shown in Figure 3.15, the dark blue measuring ball is located inside the stacking container, and the measuring radius increases with the container size.

The iso-diametral sphere naturally sinks into the accumulation container, and the change of porosity of the sphere inside the container is monitored in real time by the dark blue measurement ball.

When the particles finish the natural subsidence, the particle accumulation body is formed, and the stable porosity value of the particles in the container is finally obtained.

Different container radius values are set in turn, and the corresponding porosity stability value is obtained.

The interface of visualization results is shown in the following Figure 3.16.

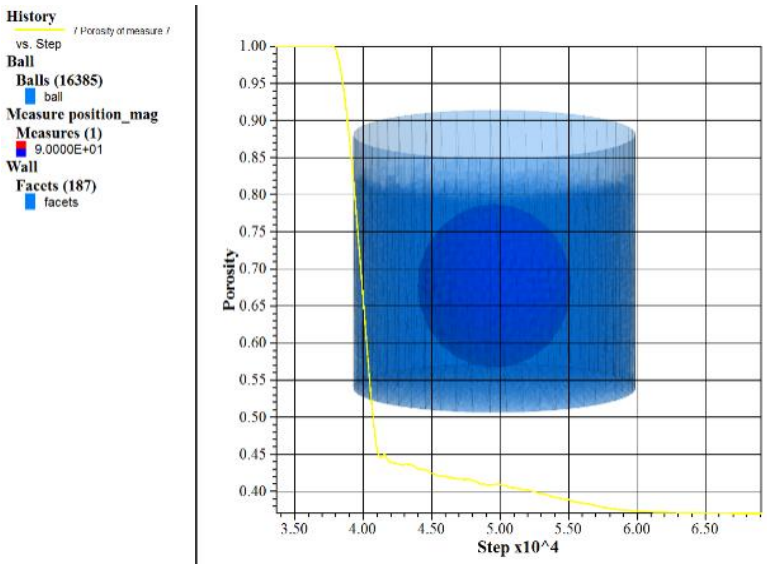

Figure 3.16 – Porosity of isodiametric sphere model

In Figure 3.16, the transparency of the iso-diameter sphere is set at 90%, so that the position of the measured ball in the barrel and the measured particle body area can be clearly observed. From the above Figure,

It can be seen that the vertical coordinate of the measured ball center is 9mm, and there is a certain interval between the measured ball and the wall of the accumulation container, in order to eliminate the influence of the boundary particles on the measured results.

2. randomly distributed sphere model (r=0.15-0.45mm) (Figure 3.17).

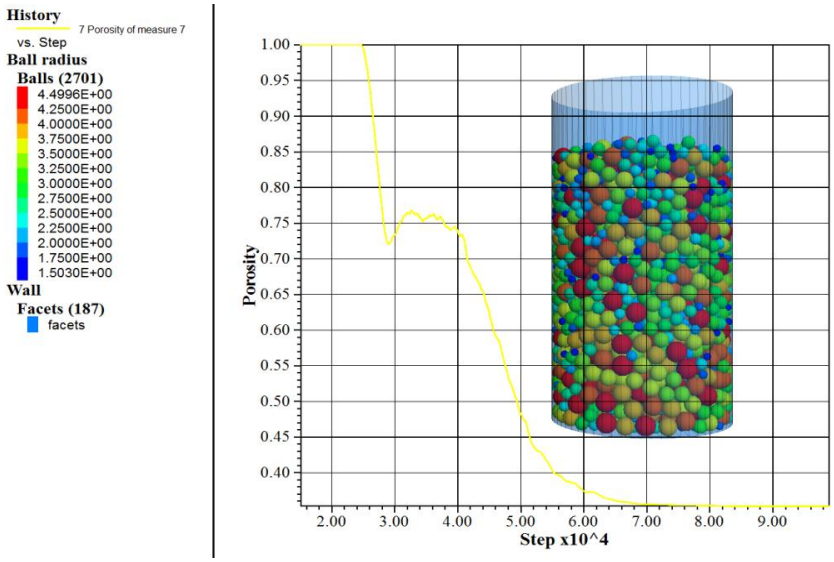

Figure 3.17 – Curve of porosity variation

As shown in Figure 3.17, the different colors of particles represent the radius of each sphere, increasing from blue to red from 0.15mm to 0.45mm successively.

The size and distribution of the sphere are shown in the Figure Different container radius values are set in turn, and the corresponding porosity stability value is obtained. The interface of visualization results is shown in the following Figure 3.18.

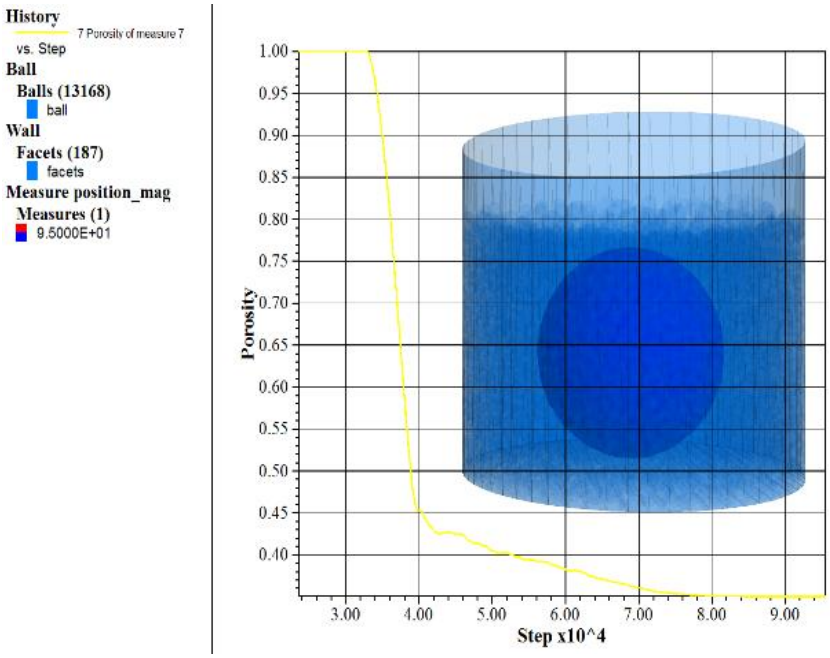

Figure 3.18 – Porosity of randomly distributed sphere model

2. normally distributed sphere model （Figure 3.19）

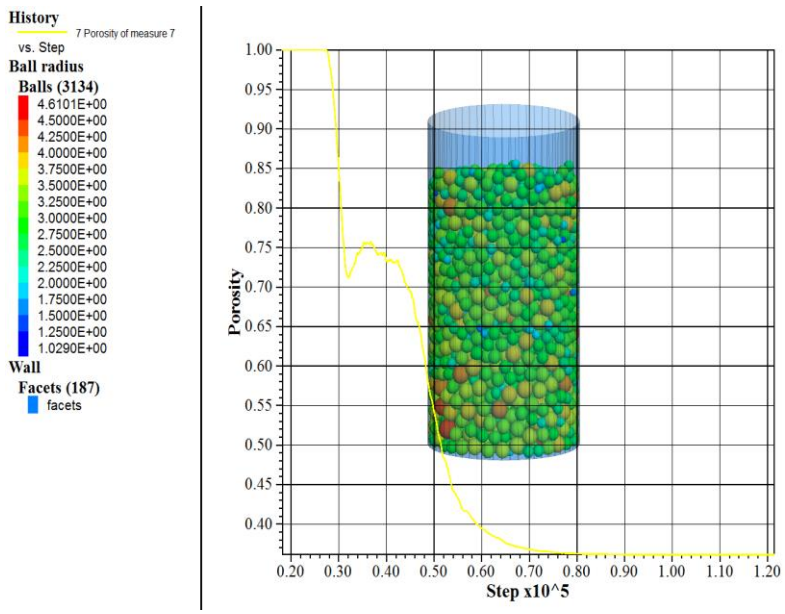

Figure 3.19 – Porosity change in sphere model

As shown in Figure 3.19, the different colors of particles represent the radius of each sphere, increasing from blue to red from 0.10mm to 0.46mm successively. The size and distribution of the sphere are shown in the Figure

Different container radius values are set in turn, and the corresponding porosity stability value is obtained. The interface of visualization results is shown in the following Figure 3.20.

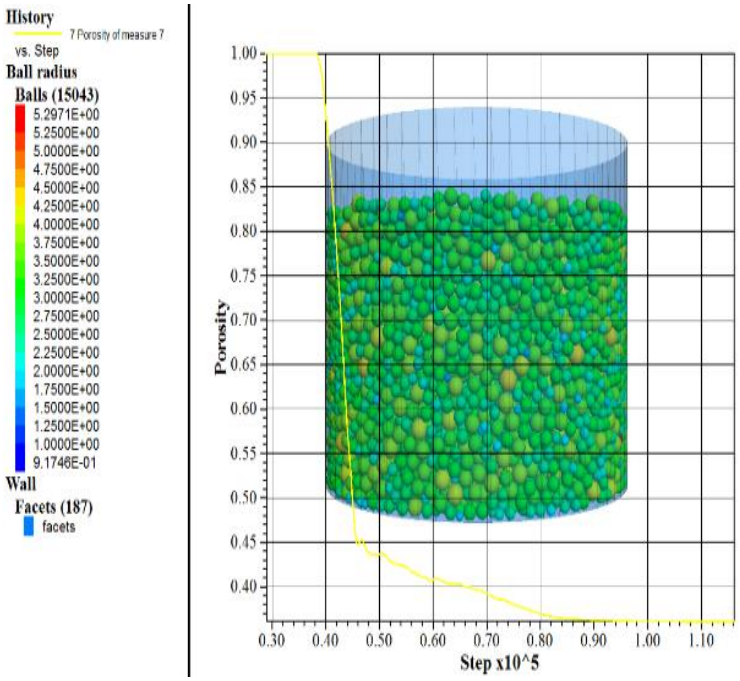

Figure 3.20 – Porosity of the normally distributed sphere model

As shown in Figure 3.20, the variation trend of the porosity change curve is roughly the same. The porosity of the measured ball in the container remains unchanged at 1 for an initial period of time, and then decreases rapidly, followed by a rise in fluctuation, and then decreases rapidly again, and finally reaches a stable value.

Whereabouts analysis the curve, the initial phase, particle has not entered the measurement inside the body, so the measured porosity data is 1, then particles into the measurement inside the body, for measuring ball fill quickly, then the sedimentation of particles are constantly through the measurements of the interior of the ball, hence porosity volatility rising trend, after measuring the ball being stacked particle effective filling, hence porosity falling fast again, finally when measuring ball covered by stacking sphere, porosity also gradually tends to the stable value.

3.4.2 Result analysis

Respectively set up random distribution sphere diameter spheres, such as particle size and particle size of normally distributed spherical particles in different size containers accumulation model, through the study, respectively each sphere model particles in different size containers are stacked porosity change trend, statistical container size effect of

different sphere model, and calculated their sphere model no size parameters of the boundary effect, at the same time, further compare the size of the sphere model parameters, draw relevant proportion coefficient, thus to provide relevant theory support production practice and scientific research.

with the size of diameter sphere as a control group the results of comparison, and according to the three principles, the generated from within 99.75% of the particle size distribution, and can be used as a random distribution sphere model control group the results of comparison, thus can be compared each other between three groups of model analysis, and convenient reasonable conclusions. Figure 3.21 is a schematic diagram of different types of sphere models.

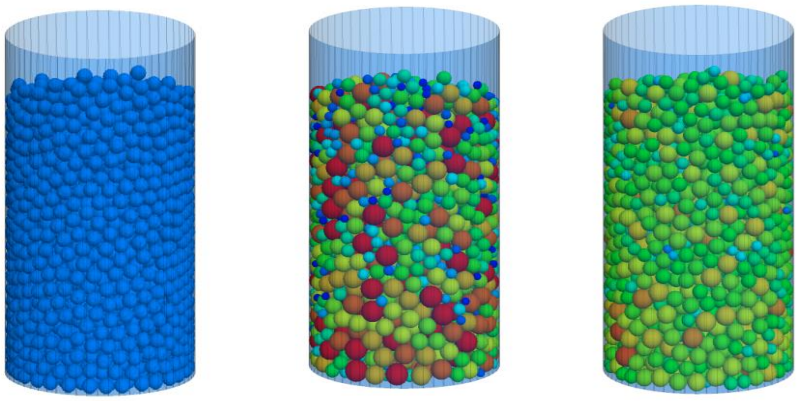

Figure 3.21 –Different types of sphere models

As shown in Figure 3.21 for sphere model for the accumulation of different types, and each of the different colors of packing containers in the grain size of the sphere radius, can be seen from the diagram, such as diameter sphere model approximation were distributed evenly in the container, arrange relatively regular wall border spheres, but, on the surface of the particles in contact with the wall of the particles have a larger gap between;

The size difference of the sphere model with random particle size distribution is large. The particle with the largest particle size is represented by red, while the particle with the smallest particle size is represented by blue. The number of both particles is relatively large, and the overall particle accumulation has a certain distribution in homogeneity.

Table 3.1 shows the porosity stability values of different sphere models in different containers sizes.

Table 3.1 –Porosity stability values of different sphere models

R, mm	2	3	4	5	6	7	8	9
r=0.3, mm	0.381	0.371	0.371	0.371	0.371	0.370	0.369	0.3705
R, 0.15-0.45mm	0.365	0.360	0.353	0.351	0.351	0.351	0.351	0.351
R, 0.25-0.35mm	0.367	0.366	0.363	0.364	0.363	0.363	0.362	0.362

As shown in Table 3.1, for different types of sphere models, the stable values of porosity in the same container size are all different, among which, the particle accumulation porosity of the iso-diameter sphere model is the largest, followed by the sphere model with normal particle size distribution, and the sphere model with random particle size distribution is the smallest.

For the iso-diameter sphere model, when the container size is greater than 3mm, that is, the size ratio between the container radius and the particle size, the influence of the container size on the boundary of the sphere particle accumulation is basically eliminated, and the porosity value is stable around 0.371. For the sphere with random particle size distribution, when the size of the container is greater than 4mm, that is, the size ratio between the radius of the container and the median particle size, the influence of the container size on the boundary of the particle accumulation of the sphere is basically eliminated, and the porosity is stable around 0.351.

For the sphere with normal particle size distribution, when the size of the container is larger than 5mm, that is, the size ratio between the radius of the container and the mean particle size, the influence of the container size on the boundary of the particle accumulation of the sphere is basically eliminated, and the porosity value is stable around 0.363.

When the size of the container is fixed, the stable value of porosity of the particle accumulation in the container from large to small is the spherical model with equal diameter, the spherical model with random particle size distribution, and the spherical model with normal particle size distribution.

4 SIMULATION AND EXPERIMENTAL DATA ANALYSIS

4.1 Simulation and experimental methods

Numerical simulation method for the discrete element method, by using the discrete particle flow visualization programming software, used for physical experiment to simulate normal particle size distribution of the function, and then carried out on the metal sphere particles size normally distributed digital modeling, through programming language control the change of the experimental parameters, the specific conditions for the simulation and purpose, and by the visual images and the chart to display the results.

The mathematical characteristics of the particle models involved in the numerical simulation should be as similar as possible to those used in the actual physical experiments. Mathematical expression for the same particle size, however, normally distributed spherical particles, because of the generation of particles is random, so every time the simulation of the particle size, the particle size of particles produced great probability of both the number of different, and the generated particles model free distribution distributed disorderly in the container, therefore, although the particle model, the mathematical expressions of the same, but the initial density and the density of the after the simulation at the end of the big probability is different, so many times for the same model need to simulate the averaged.

Physical experiments, reasonable design and manufacture of three-dimensional vibration platform that could satisfy the requirement of experiment, and the typical particle size is approximately normal distribution sphere particles mechanical vibration experiments, experimental method, control the variables in the process of repeated experiments for experiment under the same parameters and averaging, eliminating outliers and reasonable results, to the experimental results of different parameters under the horizontal comparison, and the analysis results of numerical simulation in the process validation. In this chapter, the object of study is determined as the density of spherical particles with normal particle size distribution.

4.2 Study on the packing density of spherical particles

4.2.1 Setting of initial conditions

The relevant influencing factors and variables in the numerical simulation are set as follows:

1. Cylindrical boundary container is adopted, and the inner diameter of the container is compared with the diameter of the ball, so as to eliminate the influence of boundary size as much as possible.

2. The measuring ball used to measure the particle density inside the container should be kept at a certain distance from the wall of the container, so as to eliminate the influence of the surrounding walls on the particle accumulation density inside the container as much as possible.

3. Adopt the method of overall feeding, and set the connection model between the

sphere and the sphere and the connection model between the sphere and the wall as the linear elastic model.

4. The values of the normal and tangential stiffness between the sphere and the sphere are the same.

5. The friction coefficient between the spheres is 0.015, and the damping ratio is 0.2.

6. A measuring ball with a radius smaller than the inner diameter of the charging barrel is set at the outlet of the charging funnel, and the same measuring ball is set at the top and bottom of the charging barrel for numerical simulation and software simulation.

7. The number of random seeds was set to be large enough to ensure the consistent distribution of particles in each verification experiment. In this paper, the number of random seeds was 10001.

8. The physical time of each numerical simulation and simulation is set to 30s, and the program automatically determines the time step according to the complexity of the calculated model.

4.2.2 Simulation process

1. Modeling and model response

First by FISH language program command, the solution domain, particles, wall body and ball porosity measurement, then delete the discharging mouth block plane by the program, let the ball from the funnel of natural sedimentation to cylinder barrel, the settlement of particles in the steady state, eventually convenient read the final in porosity curves measured values. The natural sedimentation process of particles is shown in the following Figure 4.1.

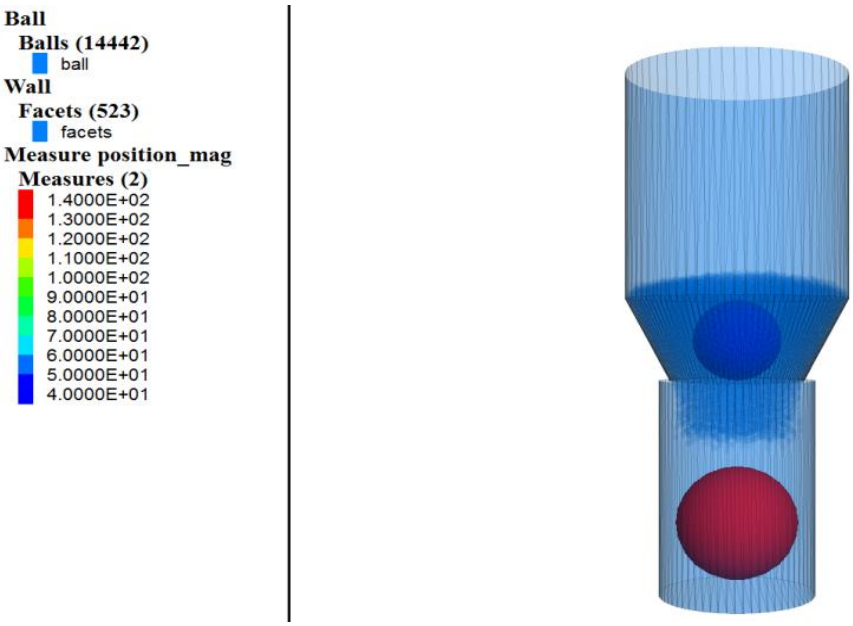

Figure 4.1–Schematic diagram of natural sedimentation of spherical particles

As the Figure 4.1, In the above simulation process, the initial parameters are set as described above. The response of the model is observed and adjusted through the visual

window, and a reasonable solution step and time can be set according to the operating state of the system.

2. Data detection

At the same time of preparing the filler, a porosity measurement ball is set at the outlet of the funnel barrel and the inside of the material barrel through the program control command, which is used to measure the porosity change curve of the ball particles at the outlet and inside the material barrel during the falling process of the ball.

The porosity measurement ball size and position are shown in the following Figure 4.2.

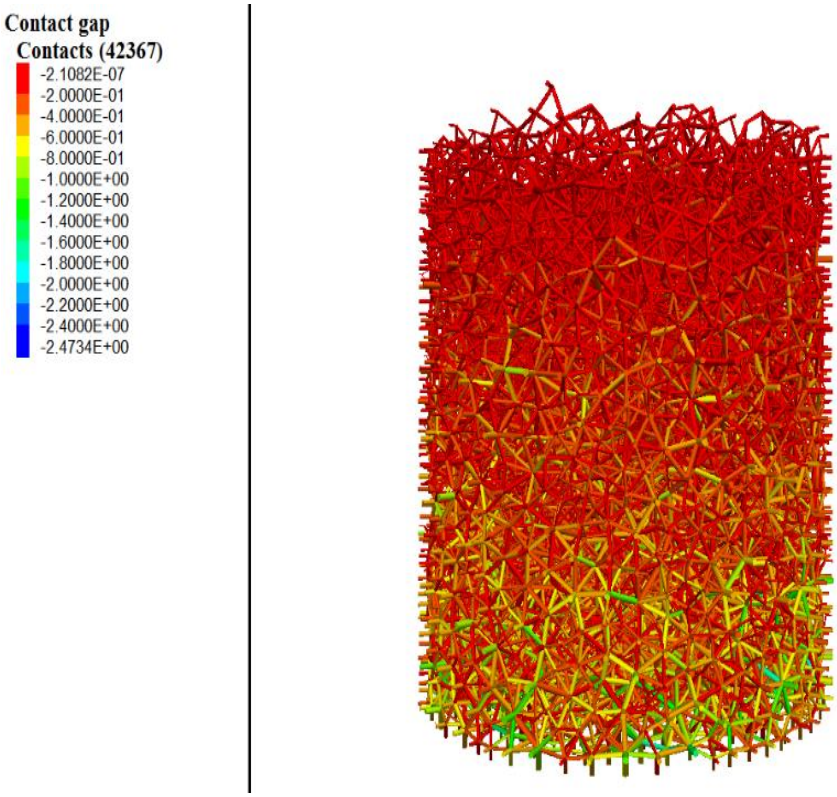

Figure 4.2 – Distribution of porosity measurement spheres

As shown in Figure 4.2, the vertical coordinate of the measuring ball set at the discharge port is 4mm and the diameter of the measuring ball is 8mm. A measuring ball with a larger radius is set inside the barrel to reduce the influence of local abnormal accumulation on the porosity value. The main porosity measurement ball is set inside the barrel, the barrel radius is 7mm, the average particle size of the ball is 0.3mm, the ratio of the two radius is about 23:1, which can effectively eliminate the influence of the boundary on the particle accumulation. Meanwhile, in order to further avoid the influence of the boundary effect on the measurement results, 1mm space is left between the measurement ball and the wall. Through the reasonable setting of the measuring ball, the real-time monitoring of porosity in the process of particle accumulation can be realized. Figure. 4.3 is the mass distribution of spherical particles, while Figure. 4.4 is the radius distribution of spherical particles.

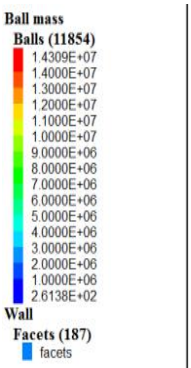

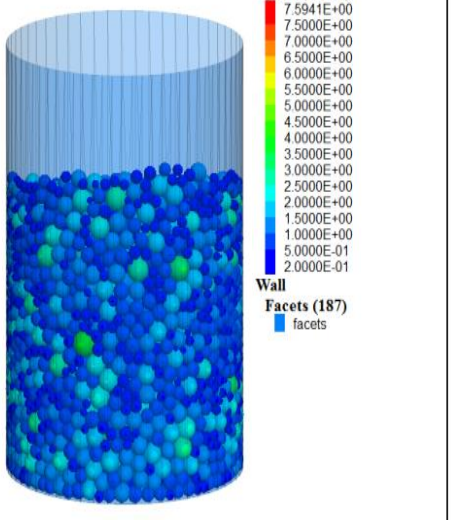

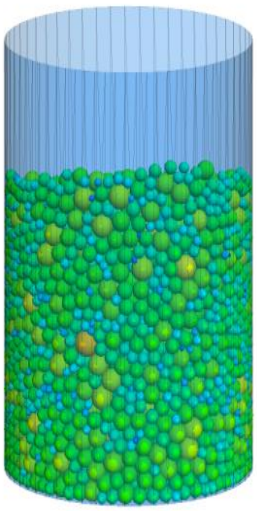

Figure 4.3 – Distribution of mass Figure 4.4 – Distribution of radius

As shown in Figure 4.3 and Figure 4.4, the distribution of the mass and radius of the spherical particles in the container after stacking is completed, respectively.

As for the spherical particles, the mass of the accumulated particles belonging to the same material property is positively correlated with the particle size, that is, the larger the particle size is, the greater the mass of the corresponding spherical particles is, so the distribution law is the same. Figure. 4.5 is a schematic diagram of the distribution of contact forces between particles in the sphere.

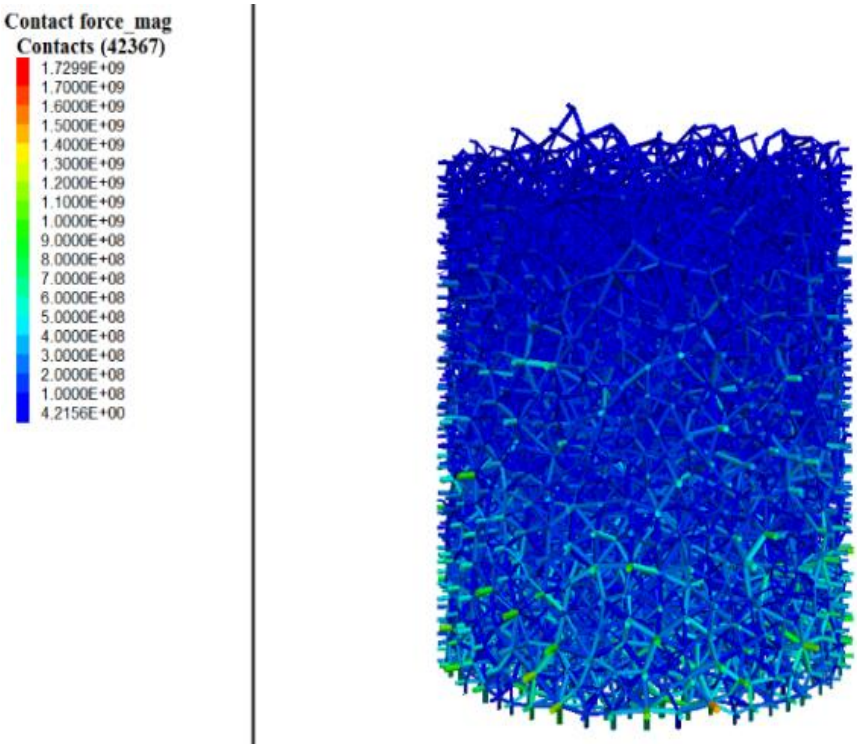

Figure 4.5 – Contact force distribution among particles

Figure 4.5 shows spheres the size of the contact force between particles distribution, because the deposit of the lower particles not only inherit the role between adjacent particles, also from upper particles under gravity, in a container near the wall of contact force between particles and wall body to balance the internal contact force between particles to produce, therefore, the size of the contact force distribution from top to bottom, from the inside out, in turn, the trend of increase, in the sphere - wall contact type compared with sphere - ball contact type of contact force is larger. In the sphere-wall contact type, the contact forces are relatively large. Figure. 4.6 is the contact gap between spheres.

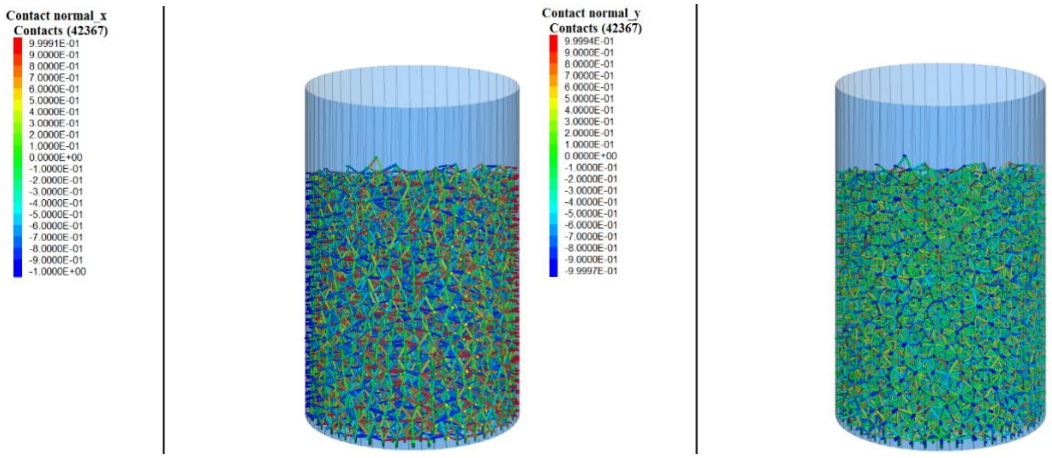

Figure 4.6 – Contact gap between spheres

Figure 4.6 said sphere, the contact between the clearance of every contact point where the dependent variable, as can be seen from the diagram, each contact point are varying degrees of overlap, the rigidity of the particles and particle body of the vertical coordinates of contact gap is larger, when the sphere stiffness must be accumulated particles from top to bottom contacts should be variables showed a trend of increase gradually, because contact as the amount of overlap, so negative. Figure. 4.7 shows the component values of the contact vector on the X and Y axes.

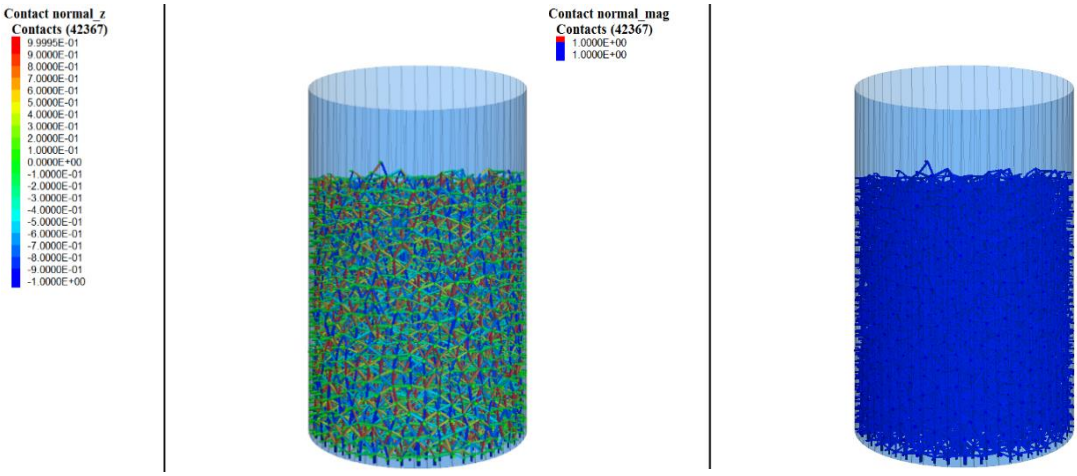

Figure 4.7 – Component values of the contact vector

In the simulation process Figure 4.7, the packing simulation was carried out for the spherical particles with normal particle size distribution.

In this paper, the influence of the spherical particles with different variances on the packing density under the same particle size mean was studied by changing the normal distribution function of particle size.

When only the normal distribution function of particle size is changed, the physical structure and mechanical properties inside the accumulation body are basically the same, and the porosity measurement ball is set at a reasonable position inside the container, so as to realize the real-time monitoring of the porosity inside the accumulation body.

For deposit, the quality of a sphere particles distribution and particle size distribution, contact types are divided into sphere - wall and the ball - sphere, the size of the contact force is not only related to the contact type, and the position of the sphere of the Z axis direction, a general from top to bottom, from the inside out, in turn, the trend of increase, because the contact point of the dependent variable is negative, so the size of the corresponding contact force is inversely proportional to the contact clearance, vector distribution and accumulation of the whole contact is consistent with the distribution of contact force, overall stability, the contact type for each axis up a greater influence on the size of the vector.

4.2.3 Porosity measurement

The packing density of sphere particles with normal particle size distribution was studied, and the mean particle size was set to 3mm to detect the change of particle porosity under different variances. The modeling, model response, porosity detection process, time steps and parameter setting were all consistent with the above verification process, and only the distribution of generated particles was changed. Figure 4.8 shows the variation curve of porosity under different particle size distributions.

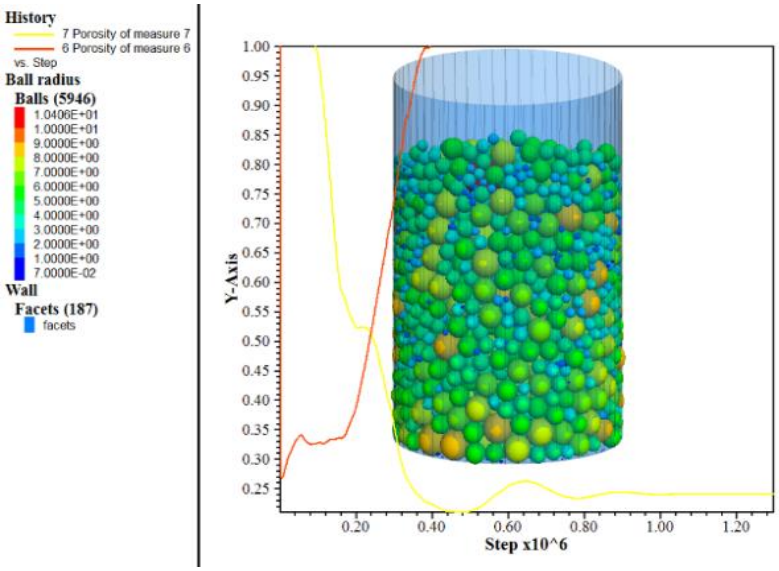

Figure 4.8 – Variation curves of porosity under different particle size distributions

As shown in Figure 4.8, the vertical axis represents the porosity value of particle accumulation, and the horizontal axis represents the time step of particle calculation. Different particle distribution states require different time steps due to the difference in internal calculation amount, but the physical time is fixed at 30s.

Red curve P6 said feeding mouth granules porosity curves, yellow curve P7 said the granule porosity curve of internal cylinder, cylinder of color represents different particles in particle size, the distribution of sphere by sphere, according to a color change under different particle size can be intuitive sphere particles deposit distribution characteristics of different variance, with the increase of the variance, the differentiation of the grain size gradually obvious, granular particle size within the gap increases gradually.

4.2.4 Results analysis

The above data are counted and the interpolation function is used for numerical analysis, with the increase of variance, the porosity first decreases and then increases, and the increase trend is obvious, indicating that when the particle size distribution exceeds a certain situation, the porosity increases rapidly. At the same time, in terms of the contrast of porosity, the porosity distribution of spherical particles with normal particle size distribution is lower than that of isodiametric spheres with the same particle size mean, so it can be concluded that the packing density of reducing spheres is generally higher than that of isodiametric spheres. With the increase of variance, for spherical particles with normal particle size distribution, the packing density first increases, then decreases, and there is a maximum packing density, and when the variance of particle distribution is greater than the value of maximum packing density, the porosity increases rapidly.

4.3 Comparison of experimental data results

According to the spherical particle accumulation characteristics in the aforementioned numerical simulation state, iron powder with particle size mean of 0.3mm, particle size normally distributed and variance of about 0.2 was selected as the experimental material in this paper, and the physical experiment was conducted through the aforementioned experimental equipment.

Found in the experimental stage, vertical direction vibration will cause great influence to the stability of the particle accumulation, not conducive to the formation of grain body density, thus provide only the vibration of the horizontal plane, at the same time, in a horizontal plane dimension in the direction of vibration, the vibration force can good between the particles of the container body diffusion, the accumulation of particles during the vibration effect than two-dimensional vibration effect, at the same time in order to avoid the X, Y direction because of the exciting force size different from unnecessary displacement of particle collision, set the horizontal direction is consistent with the amplitude and frequency of the vibration motor.

Through the method of control variables, with the increase of amplitude, tso that the granularity after vibration can reach the relative density accumulation.

At the same time, the longitudinal comparison of Figure a to Figure g shows that for the matching parameters of different frequencies and amplitudes, when the vibration frequency is 25Hz and the amplitude is about 0.1mm, the porosity of the particle body can reach a relative minimum value of about 0.136, that is, the bulk density of the particle body reaches a maximum value of 0.864.

As can be seen from the trend of the curve in the Figure, with the increase of vibration frequency, the value of the optimal amplitude matching parameter gradually decreases, because for the vibration system, the vibration intensity is generated by the joint action of vibration frequency and amplitude, and when the vibration intensity must be, the vibration frequency is inversely proportional to the amplitude.

4.4 Chapter summary

The content mainly studies size normally distributed packing density of sphere particles, through the analysis of the mean u = 3 mm, variance of variable porosity variation curve of sphere model, and through the linear interpolation of data from linear regression analysis, the results show that with the increase of the variance, the particle size of normally distributed spherical particles, the change trend of the porosity increase with the decrease of the first, in contrast to the trend of the change of the density.

Through data processing methods such as point selection, data analysis and curve fitting in physical experiments, it is concluded that :1. When the vibration frequency is constant, the bulk density of particles increases first and then decreases with the increase of amplitude; 2. With the increase of vibration frequency, the overall packing density of particle accumulation increases first and then decreases; 3 The vibration intensity of vibration frequency and amplitude together can describe the relationship between the two. Generally speaking, the matching parameters of the two are inversely proportional, that is, the higher the vibration frequency is, the lower the amplitude parameter of the corresponding dense accumulation.

5 USE TECHNOLOGY OF THE 3D PRINTING FOR WIND TURBINES

5.1 The analysis strong and weaknesses of technology based on the packing density study on the metal powder particles used in 3D Printing, opportunities and threats of its application for wind turbines

5.1.1 Advantages and disadvantages of 3D printing

1. Engineering manufacturing.

In terms of engineering manufacturing, on the one hand, it is the production of important parts used in high-end manufacturing such as national defense, military industry, aerospace and so on. The production of these parts has high requirements, and the traditional process is often unable to achieve or even to achieve but the cost is too high. On the other hand, small batch or single-piece production is used for engineering.

2. Civil development.

In terms of civil development, 3D printing technology is regarded as the core technology of the "third industrial revolution", bringing profound changes in manufacturing process and reducing labor costs.

3. Medical.

At the same time, 3D printing technology has also made remarkable achievements in medical treatment. It can be used to print artificial limbs and help more people who have lost their legs by accident to stand up again and live like normal people. The "3D printed heart" is another achievement that USES 3D printing technology to simulate human organs. The 3d-printed heart can be used as a copy of the heart's anatomy, making it useful for practicing complex heart surgery.

4. The construction industry.

In the construction industry, too, 3D printing has potential for more than just DIY home items. In fact, the technology could revolutionize the traditional construction industry. Compared with traditional construction industry, 3D printed buildings not only have reliable quality of building materials, but also can save 30%-60% of building materials, shorten construction period by 50%-70%, reduce labor by 50%-80%... By some estimates, printing could reduce construction costs by at least 50%, making homes more affordable. However, the new "ink" printing of the building, its stiffness, strength and durability and other comprehensive performance to be further verified.

Today, 3D printing technology still faces great challenges in creating an infinite future for us: Manufacturers don't like it. Low productivity, high cost. The high cost of 3D printing is well known. Although the cost of 3D printing is lower than before, the manufacturing cost of a single product still cannot be fundamentally solved.

The cost of making one finished product in 3D is not much different from the cost of making 10,000 finished products, and it is far higher than the average cost per finished product for a large manufacturing company in mass production. At the same time, the early investment of 3D printing technology is large and the profit margin is low, so it cannot attract a large amount of investment.

3D printing won't replace traditional productivity in the foreseeable future. SWOT-

analysis of use of technology of the 3D printing for wind turbines [32]. Table 5.1 shows the SWOT analysis.

Table 5.1 –SWOT-analysis of use of technology of the 3D printing for wind turbines

External factor / Internal factor	Strength	Weakness
	1. Complex integration molding 2. Intelligent manufacturing Short design cycle 3. Meet individual needs 4. Economize on raw materials	1. Low productivity, 2. High cost 3. High requirements on equipment 4. Product performance is unstable
Opportunities	SO	WO
1. Civil development 2. Material technology development 3. The construction industry 4. Personalized demand acceleration	1. Application of accelerated 3D printing in the high-end field of turbine blades 2.Provide efficient turbine blade design and manufacturing services 3.Provide integrated turbine blade molding service	1. Seek to reduce the cost of materials processing technology 2. 3D printing is carried out with excellent equipment 3. Design the best printing parameters to improve printing efficiency
Threats	ST	WT
1. Manufacturers don't like it 2. Design threshold 3. Difficulty of mass customization 4. Single finished product is expensive	1.3D printing makes up for the manufacturing blind spots in traditional industries 2. Develop 3D printing education	1. Learn from the latest developments in materials to reduce costs 2. Adopt advanced sensor and control technology to improve stability

As can be seen from the analysis in table 5-1, gas turbine blades are one of the key components of a gas turbine, and the quality of the components directly determines the efficiency and safety of the gas turbine.

The application of 3D printing technology in gas turbine blade manufacturing has the following advantages:

1. Using 3 D printing metal blade not only save the blade casting, forging blank and machining of complex process, and the difference between "reduced material" traditional manufacturing mode, can be formed with complicated geometry of blades products, and meet the requirement of precision and operational performance, and greatly save the production cost, shorten the product cycle.

2. The 3 D printing metal forming gas turbine blade easy to control the product manufacturing process, product dropped sharply the uncertain factors in the process of production, especially the artificial factors, the same model file with the same materials using high precision 3 D printer, the quality of the product can even is superior to the traditional manufacturing mode.

3. In the field of blade parametric design, the original blade model was parameterized and modified by CAD modeling software, and the blade products were rapidly manufactured by 3D printers to quickly adapt to the complex and changeable market demand and improve the core competitiveness of the enterprise.

4. In the field of gas turbine blade repair and manufacturing, metal 3D printing technology is adopted to repair gas turbine blades, which can increase the blade service life and reduce the cost of repair and remaking.

5. The application of 3D printing technology in investment casting can reduce the mold manufacturing time and shorten the cycle of new products. At the same time, the 3D printing blade model can be effectively controlled when used in investment casting to ensure the size requirements of investment model.

5.1.2 Application of 3D metal printing on wind turbines

Normally, when the wind passes through a turbine, almost half of the air is forced to stay around the blades instead of going through them, and the energy in those winds is lost. Conventional wind turbines can only use up to 59.3% of the wind energy, a value known as the Betzlimit. Wind turbines, designed using jet engine technology, overcome one of the fundamental drawbacks of traditional wind turbines.

A shroud around the blades of a wind turbine guides air through them and accelerates them, increasing electricity production. Wind turbines are like air intakes for a jet engine. When air enters, it first encounters a set of fixed blades, called stators, which direct the air into a set of rotating vanes called rotors.

Air pushes against the rotor and appears on the other side, allowing the air to flow more slowly than it would outside the turbine. The shelter is shaped in such a way that it directs relatively fast-moving air from the outside into the area behind the rotor. The fast-moving air accelerates the slow-moving air, turning the area behind the turbine blades into a depression to absorb more air through them. The idea of obscuring wind turbine blades is not new. Early designs were too big to be practical or performed poorly, in part because the blades had to be aligned so tightly that the wind was between 30 and 40. The new blades are smaller and work off the wind at an Angle of 150 to 200. Facing wind turbine structure and production engineers, the biggest problem is that how to implement optimization, let the wind turbine produced huge at the same time reduce the aerodynamic

noise, previous generations of manufacturing processes and materials for low consumption of largely limits the wind turbines on the production structure and purpose, but 3 D printing can fundamentally solve the problem.

The basic idea of using hybrid materials is to use materials of different mass and density at different stress points of the wind turbine blades, which can reduce the total weight of the wind turbine blades and strengthen the overall structure of the wind turbine blades. Existing examples include the use of high-modulus glass or carbon fibre to make the mesh and roots of turbine blades, where the force is greater, and the use of ordinary glass to make external structures. This saves money, optimises existing infrastructure and takes advantage of innovative technologies.

As the rotor size continues to increase, and wind turbines continue to update their existing energy efficiency and power density, 3D printing will make a special contribution in this regard. Currently, the biggest difficulty for the widespread use of wind turbines is the problem of cost. Many advanced production processes, such as 3D printing, have made many contributions to solve this problem. While hybrid materials and 3D printing are still in the development stage, these technologies will help solve structural stability, optimize aerodynamics and reduce noise as they mature.

Metal composites, for example, have been widely used in aviation for the past decade or so, and as their prices fall, they will find greater use in the wind power industry. Material innovation will be one of the most important factors to change the status quo, and technological development is bound to revolutionize manufacturing in the next two years. The problem affects the entire field of wind energy, where the material used in the blades of wind turbines can be eroded due to weather conditions. VTT's anti AGE project USES artificial intelligence and 3D printing to find a solution to the material problem.

5.2. Gantt's schedule of actions for implementation of technology based on the packing density study on the metal powder particles used in 3D Printing for wind turbines

Gant’s schedule is also known as Bar chart and Bar chart. Named after the proposer, Mr. Henry L. Gant’s [33]. The idea behind Gant’s schedules is simple, that is, to graphically represent the sequence and duration of activities for any given item by means of activity lists and time scales.

It is basically a line drawing, with the horizontal axis representing the time, the vertical axis representing the activities (projects), and the line representing the planned and actual completion of the activities over the entire period. It visually shows when the task is planned and how the actual progress compares to the planned requirements [34]. This makes it easy for managers to figure out what remains of a task (project) and to assess progress.

The Gant’s schedule was one of the earliest attempts to relate activities to time for the purpose of job sequencing. This diagram can help enterprises to describe the use of resources such as work centers, overtime work, and so on. A Gant’s schedule chart can be used to check work progress. It indicates which work was completed on time, ahead of

schedule, or behind schedule. Gant's schedules can also be found in practice for a variety of purposes. According to the process of metal 3D printing, the following Gant's chart is made. The main components are the manufacturing of wind turbine blades [35].

The gant's schedule in table 5.2 is an action plan for implementing wind turbine technology.

Table 5.2– Gantt's schedule of actions for implementation of technology for wind turbines

Research and Project stages	Performers	Period of implementation of the project 2019 - 2020, month								
		9	10	11	12	1	2	3	4	5
1	2	3								
1. Development of introduction.	S. Li									
2. Literature search at home and abroad.	S. Li									
3. Study and use of 3d drawing software	S. Li									
4. Design 3d vibrating table	S. Li									
5. Analysis 3D model	S. Li									
6. 3D printer selection	S. Li									
7. SWOT-analysis and Gant's schedule	A. Alabugin S. Li									
8. Prepare PPT	A. Alabugin R. Alabugina S. Li									
9. Finish final thesis	A. Alabugin R. Alabugina S. Li									
10. Registration of SUSU TW	R. Alabugina S. Li									

As shown in the table 5.2. In this section, I have drawn a gantt diagram for the entire article. Gantt diagram shows the whole process of my paper. Project determination, model design, model analysis, experimental environment preparation, experimental experiments, experimental results analysis, PPT production.

Aiming at the need of shortening the period of research and development of gas turbine blades, in this paper the current mainstream 3 D printing technique and its molding principle, on the basis of metal 3 D printing technology at home and abroad is expounded for gas turbine blade manufacturing and using laser cladding technology rapid repair of research status and applications of blade, metal is analyzed compared with the traditional manufacturing technology of 3 D printing technology advantage, 3 D printing technology

for gas turbine blade are introduced the research progress of investment casting. The results show that 3D printing technology has a broad application prospect in the field of gas turbine blade rapid manufacturing.

5.3 Conclusion

The material in the blades of wind turbines can be eroded, a problem that affects the entire wind energy sector. 3D printing is the solution to the material problem. Erosion of the blade material due to rain, hail and dust has greatly reduced the life of wind turbines, which are expensive to replace and lose 2-4% of the value generated by wind power.

The problem wastes billions of euros and adds an extra cost to wind power. As the size of wind turbines increases and wind farms are increasingly placed offshore, the importance of addressing this problem has increased in the face of increasingly demanding conditions." There are many alternatives to the materials used in wind turbine blades, and one needs to find the most suitable one among all the alternatives. Using artificial intelligence, it is possible to find a specific material solution for a product, but it is very difficult to make such highly customized materials using traditional manufacturing techniques. 3D printing can solve this problem by making products of any shape with the desired materials.

To decrease the development cycle of blades of gas turbine, the present research situations as well as the application both at home and abroad of metallic three-dimensional printing technology used in the fields of rapid manufacture and the repairment method of laser cladding technology for gas turbine blades are elaborated on the basis of summarizing the main three-dimensional printing technology and its forming principle at present. The advantage of metallic three-dimensional printing technology compared with the traditional manufactural technology. The research progress of three-dimensional printing technology in investment casting fields to manufacture gas turbine blades is introduced. The result shows that the three-dimensional printing technology has broad application prospects in the fields of rapid manufacture of blades for gas turbine.

6 CONCLUSION AND PROSPECT

6.1 Conclusion

In this paper, the discrete element method is adopted to sphere particles of numerical simulation for the process of accumulation, using physical experiment used metal powder's particle size distribution function fitting sphere particles normal distribution model of the best, and numerical simulation, the numerical simulation results are comparative analysis of implementation of complex metal powder particle size normally distributed high density accumulation, corresponding matching parameters are obtained.

Is the key to establish the appropriate particle accumulation model, particle size distribution was approximate normal distribution density of metal powder particles optimal value, through the discrete particle flow yuan visual programming software to establish a normal distribution model of discrete element granules of normally distributed particle size, the density of sphere particles were characterized with dynamic analysis, the stress of the precise characterization of particulate matter accumulation process, motion, arrangement, etc., will be the result of numerical simulation, this paper compares and analyzes the conclusion of the normal distribution, the density of sphere particles main influence factors, studying the characteristics of its density.

For spherical particles with normal particle size distribution, the packing density is generally higher than the theoretical value of 0.7406. The change curve of porosity of particles with mean value of 0.3mm and variable variance was analyzed, and the data obtained were linearly regressed. The results showed that the porosity first decreased and then increased with the increase of variance, which was contrary to the change trend of density.

Compared with Horsfield compacting theory, the packing density of sphere particles with normal particle size distribution is generally between 0.7406 and 0.793 for the theoretical value of first-order ball and second-order ball, and when the mean value of the sphere particle model is 0.3mm and the variance is 0.2, the packing density reaches a maximum of 0.795, which is slightly higher than that of the second-order ball.

For sphere particles with normal particle size distribution, with the increasing of the stiffness value of the sphere particles, when the stiffness value $K \geqslant 5e9$, the particle accumulation density tends to 0.346. The porosity of particle accumulation in the accumulation container generally increases first and then becomes stable. When the stiffness value $K \leqslant 1e10$, the growth trend is faster; when the stiffness value $K \geqslant 1e10$, the growth trend is basically stable, and finally approaches the stable value 0.345. By comparing and analyzing the stable values of porosity of different measurement balls, it can be concluded that when $K \leqslant 1e10$, the porosity of particle accumulation is negatively correlated with the accumulation depth. In general, with the increase of particle stiffness, the porosity of particle accumulation first increases rapidly, then fluctuates steadily, and finally tends to 0.345.

For the sphere model with the same particle size distribution, the porosity of the particle accumulation decreases with the increase of the container size. When the container

size is larger than a certain critical value (the values of the sphere model with different particle size distribution are not equal), the porosity of the particle accumulation basically remains unchanged.

The size ratio between the container radius and the mean particle size of the isopod sphere model is greater than 10, and the porosity is stable at about 0.371. The size ratio of the median particle size of the sphere model with random particle size distribution is greater than 14, and the porosity is stable at about 0.351. The size ratio of the mean particle size of the sphere model with normal distribution of vessel radius and particle size is greater than 17, and the porosity is stable at about 0.363. When the size of the container is constant, for the spherical particle accumulation model with different particle size distribution but the same particle size mean, the stable value of porosity of the iso-diameter sphere model is the largest, indicating that the porosity of the mixed particles can be effectively reduced. Sphere particles in particle size normally distributed physical vibration test available: when a certain vibration frequency, particle packing density body along with the increase of amplitude decrease after rising first, and with the increase of vibration frequency, the density of particle accumulation integral accumulation rise after the first reduce the trend, in general, for the same distribution of particles, when the higher the vibration frequency, the amplitude of the corresponding density parameters is lower.

The material in the blades of wind turbines can be eroded, a problem that affects the entire wind energy sector. 3D printing is the solution to the material problem. Erosion of the blade material due to rain, hail and dust has greatly reduced the life of wind turbines, which are expensive to replace and lose 2-4% of the value generated by wind power. In this paper, through the development of Gant's schedule, I reasonably arranged my task plan, and finally completed the research on metal powder 3D printing technology in turbine blades. For its specific application, its advantages and disadvantages are analyzed and compared through SWOT table, from which it can be seen that the design of 3D printing process parameters needs to be further improved and the performance of metal 3D printer is also required to be higher.

6.2 Outlook

The spherical particle accumulation model with normal particle size distribution still needs continuous simulation and verification. Due to the randomness of particle size distribution and the complexity of calculation process, it is easy to generate errors in each simulation process due to the differences in computer performance and programming.

Follow-up research and work are as follows:

1. Establish the corresponding relationship between powder particle accumulation and defects of 3D metal printed parts, predict defects, and realize reasonable control of defects of parts.

2. This project mainly USES PFC5.0 as a simulation method, which requires further optimization of programming statements, enhancement of model accuracy, reasonable optimization of particle contact model, boundary conditions, definition of material properties, random distribution state and other properties.

3. Using the computing power of more powerful server for larger particles simulation

research, by expanding the number of particles body, accelerate the particles between speed and accuracy, as far as possible to eliminate the individual particles randomly distributed on the whole the impact of bulk density, and makes the simulation result closer to actual accumulation of particles.

4. In this paper, the particle size of normally distributed particles with a large number of simulation research, but the lack of corresponding simulation model of the physical experimental material to compare, we still lack of specific sphere of particle size distribution of particles produced in the body and high precision of granular materials preparation, thus how to improve the ability of the preparation of spherical powder particles also need further research topic.

5. With advances in science and technology, the market for gas turbine blade of product precision, service life, maintenance way, put forward the more stringent requirements, efficiency of 3 D printing technology applied in leaf development and manufacturing, to adapt to the high reliability, high life, lightweight, low cost and rapid response to market demand, must quickly to advanced gas turbine blade manufacturing have a profound impact.

REFERENCES

1 Jaeger, H.M. Granular solids, liquids, and glasses / H.M. Jaeger, S.R. Nagel, R.P. Behringer // Mod. Phys. -1996. -P. 1259-1273.

2 Bideau, D. Disorder and granular media, random materials and process, Ed. H.E. Stanley and E / D. Bideau, A. Hansen and Guyon // Elsevier Science Publishers. -North-Holland, Amsterdam. - 1993. -P. 67-72.

3 Bernal, J.D. Coordination of randomly packed spheres / J.D. Bernal and J. Mason // Nature. - 1960. - P. 910-911.

4 Bernal, J.D. Optimization of multi-component hard sphere liquids with respect to dense parking / J.D. Bernal // Proc. Roy. Inst. -1959. - P. 37-39.

5 Scott, G.D. On random packing of spheres / G.D. Scott, A.M. Charles, M.K. Mark // Phys. -1964. -P. 611-613.

6 Finney, J.L. Random packing and the structure of simple liquids / J.L. Finney, A. Soc. Lond // Proc. Roy. -1970. - P. 479-493.

7 Smith, W.P. Packing of homogeneous spheres Foote / W.P. Smith and B. Sang // Physical Review. - 1929. - P. 1271-1274.

8 Bernal, J.D. Geometrical approach to the structure of liquids / J.D. Bernal // Nature. -1959. - P. 141-147.

9 Mehta, A. Vibrated powders-a microscopic approach / A. Mehta, G.C. Barker // Phys. Rev. Lett. - 1991. - P. 394-397.

10 Barker, G.C. Vibration powder: structure, correlation, and dynamics / G.C. Barker, A. Mehta // Phys. Rev. Lett. - 1992. - P. 3435-3446.

11 Philippe, P. Compaction dynamics of a granular medium under vertical tapping / P. Philippe, D. Bideau // Europhys Lett. - 2002. - P. 677-683.

12 Yang, R.Y. Simulation of the packing of cohesive particles / R.Y. Yang, R. Zou, K. Dong // Computer Physics Communications. - 2007. - P. 206-209.

13 O'Hern, C.S. Random packing of frictionless particles / C.S. Ohern and S.A. Langer // Phys. Rev. Lett. - 2002. - P. 1-4.

14 Tai, C.H. Dynamic behaviors of powders in a vibrating bed // C.H. Tai, S. S. Hsia // Powder Technol. - 2004. - P. 221-232.

15 Berryman, J.G. Random close packing of hard spheres and disks / J.G. Berryman // Phys. Rev. A. - 1982. - P. 1053-1061.

16 Stachurski, Z.H. Definition and properties of ideal amorphous solids / Z.H. Stachurski // Phys. Rev. Lett. - 2003. - P. 1-4.

17 Luding, S. Granular materials under vibration: simulations of rotating spheres / S. Luding // The American Physical Society. - 1995. - P. 4442-4457.

18 Levin, Y. Crystallization of hard spheres under gravity / Y. Levin // Physical. - 2000. - P. 100-104.

19 Bernal, J.D. Growth of crystal from random close packing / J.D. Bernal, K.R. Knight and I. Cherry // Nature. -1964. - P. 852-855.

20 X, An. Effect of vibration conditions and material friction on dense packing of vibrated equal spheres / X. An // Powder Technol. - 2008. - P 102-109.

21 Cheng, Z.D. Phase diagram of hard spheres / Z.D. Cheng, P.M. Chaikin, W.B. Russel et al // Material sand Design. - 2004. - P. 34-36.

22 Aste, T. Investigating the geometrical structure of disordered sphere packings / T. Aste, M. Saadatfar, A. Sakellariou et al // Physica A: Statistical Mechanics and its Applications. - 2004. - P 16-23.

23 Echt, O. Magic numbers for sphere packings: experimental verification in free xenon clusters / O. Echt, K. Sattler, E. Recknagel // Physical Review Letters. - 1981. -P. 1121-1124.

24 Anand, A Predicting discharge dynamics from a rectangular hopper using the discrete element method (DEM) / A. Anand, J.S. Curtis, C.R. Wassgren et al // Chemical Engineering Science. - 2008. - P. 5821-5830.

25 Cleary, P.W. DEM modelling of industrial granular flows: 3D case studies and the effect of particle shape on hopper discharge / P.W. Cleary, M.L. Sawley // Applied Mathematical Modelling. - 2002. - P. 89-111.

26 Hbhner, D. A numerical study on the influence of particle shape on hopper discharge within the polyhedral and multi-sphere discrete element method / D. Hbhner, S. Wirtz, V. Scherer // Powder Technology. - 2012. - P. 16-28.

27 X, An. Experiments on densifying packing of equal spheres by two-dimensional vibration / X. An, C. Li // Particuology. - 2013. - P. 689-694.

28 X, An. Experimental study of the packing of mono-sized spheres subjected to one-dimensional vibration / An. X, C. Li, R.Y. Yang, et al // Powder Technology. - 2009. - P. 50-55.

29 Cundall, P. A program to model granular media using the distinct element method / P. Cundall // Technical note. - 1978. - P. 344-354.

30 Cundall, P. A discrete numerical model for Geo-technique / P.A. Cundall, O.D. Strack // Technical note. - 1979. - P. 47-65.

31 Strack, O. Cundall P A. The distinct element method as a tool for research in granular media / O. Strack //Department of Civil and Mineral Engineering. University of Minnesota. - 1978. - P. 55-62.

32 Ellenberger, J. Counter-current operation of structured catalytically packed distillation columns pressure drop, holdup and mixing / J. Ellenberger // Krishna R. Chemical Engineering Science. - 1999. - P. 39-45.

33 Humphrey, W. VMD: Visual molecular dynamics / W. Humphrey, A. Dalke, K. Schulten // Journal of Molecular Graphics. - 1996. - P. 33-38.

34 Cundall, P. A program to model granular media using the distinct element method / P. Cundall // Technical note. - 1978. - P 123-125.

35 Cundall, P.A. A discrete numerical model for granular assemblies / P.A. Cundall, O.D.L. Strack // Geo technique. - 1979. - P. 47-65.

THANKS

This topic is completed under the careful guidance of my tutor, and I have made some guiding Suggestions and recommendations for the research direction of my thesis.

In the process of writing the paper, I timely gave careful guidance to the difficulties and doubts I encountered, put forward a lot of Suggestions for improvement, and invested a lot of effort and energy.

Here I would like to express my sincere thanks to A.A. Alabugin for his help and care.